Current Biology 20, 2199–2206, December 21, 2010 ©2010 Elsevier Ltd All rights reserved DOI 10.1016/j.cub.2010.11.038

Report

Acute Induction of *Eya3* by Late-Night Light Stimulation Triggers *TSH*β Expression in Photoperiodism

Koh-hei Masumoto,[1,3] Maki Ukai-Tadenuma,[1] Takeya Kasukawa,[2] Mamoru Nagano,[3] Kenichiro D. Uno,[2] Kaori Tsujino,[1,4] Kazumasa Horikawa,[3] Yasufumi Shigeyoshi,[3,*] and Hiroki R. Ueda[1,2,4,5,*]

[1]Laboratory for Systems Biology
[2]Functional Genomics Unit
RIKEN Center for Developmental Biology, 2-2-3 Minatojima-minamimachi, Chuo-ku, Kobe, Hyogo 650-0047, Japan
[3]Department of Anatomy and Neurobiology, Kinki University School of Medicine, 377-2 Ohno-Higashi, Osakasayama City, Osaka 589-8511, Japan
[4]Graduate School of Science, Osaka University, 1-1 Machikaneyama, Toyonaka, Osaka 560-0043, Japan
[5]Department of Mathematics, Graduate School of Science, Kitashirakawa Oiwake-cho, Sakyo-ku, Kyoto, Kyoto University, Kyoto 606-8502, Japan

Summary

Living organisms detect seasonal changes in day length (photoperiod) [1–3] and alter their physiological functions accordingly to fit seasonal environmental changes. *TSH*β, induced in the pars tuberalis (PT), plays a key role in the pathway that regulates vertebrate photoperiodism [4, 5]. However, the upstream inducers of *TSH*β expression remain unknown. Here we performed genome-wide expression analysis of the PT under chronic short-day and long-day conditions in melatonin-proficient CBA/N mice, in which the photoperiodic *TSH*β expression response is preserved [6]. This analysis identified "short-day" and "long-day" genes, including *TSH*β, and further predicted the acute induction of long-day genes by late-night light stimulation. We verified this by advancing and extending the light period by 8 hr, which induced *TSH*β expression within one day. In the following genome-wide expression analysis under this acute long-day condition, we searched for candidate upstream genes by looking for expression that preceded *TSH*β's, and we identified the *Eya3* gene. We demonstrated that *Eya3* and its partner *Six1* synergistically activate *TSH*β expression and that this activation is further enhanced by *Tef* and *Hlf*. These results elucidate the comprehensive transcriptional photoperiodic response in the PT, revealing the complex regulation of *TSH*β expression and unexpectedly rapid response to light changes in the mammalian photoperiodic system.

Results and Discussion

Genome-wide Expression Analysis of the Mouse Pars Tuberalis under Chronic Conditions

The pars tuberalis (PT) is thought to be responsible for detecting photoperiod, by integrating circadian time and environmental light/dark information [7–9]. Recently, a genome-wide expression analysis revealed that the thyroid-stimulating hormone (TSH) pathway triggers photoperiodic responses in the Japanese quail [4, 5]. In mammals, nocturnal melatonin secretion is thought to carry environmental light/dark information to the PT [10–14], where the melatonin receptor is highly expressed [15]. However, the detailed molecular mechanism that links melatonin signals with *TSH*β expression in the PT remains unclear.

To identify the upstream inductive mechanism of *TSH*β expression, we performed genome-wide expression analyses of the PT under chronic short-day and long-day conditions in melatonin-proficient CBA/N mice, in which the photoperiodic *TSH*β expression response is preserved [6] (Experimental Procedures). The data obtained were first analyzed for circadian gene expression (see Supplemental Experimental Procedures available online) because PT contains circadian oscillators [16] (Figure S1A; Supplemental Results and Discussion). We identified 1000 significant 24 hr rhythmic genes in the PT (Figure 1A; Table S1). The identified genes included several clock and clock-controlled genes (Figure 1B; Table S2; Supplemental Results and Discussion). Their average peak time in the long-day condition was 7.71 hr later than in the short-day condition (Figure 1B), suggesting that circadian clocks in the PT are entrained to the end of a light period.

The obtained data were next analyzed to identify "photoperiodic" genes in the PT (Supplemental Experimental Procedures). This photoperiodic expression analysis significantly identified 246 "long-day" genes and 57 "short-day" genes in the PT (Figure 1C; Table S3). The identified genes included *TSH*β, which was further confirmed by quantitative PCR (qPCR) and radioisotope (RI) in situ hybridization (Figure 1D). In contrast, *TSH* α subunit (*Cga*) and *Tac1* [17] did not respond to the photoperiod in the mouse PT (Figures S1B and S1C; see details in Supplemental Results and Discussion).

Late-Night Light Stimulation Immediately Induces *TSH*β Expression in the Mouse PT

We next examined the timescale of the *TSH*β induction after the transition from the short-day to the long-day condition. We transferred mice from the short-day to the long-day condition by delaying lights-off for 8 hr (hereafter, the "delay" condition) and sampled the PTs at zeitgeber time 16 (ZT16; ZT0 was defined as the time of lights-on) because *TSH*β is rapidly induced at around ZT16 in the PT of the Japanese quail [4]. However, in contrast to the previously reported immediate induction of *TSH*β in the quail, *TSH*β expression in the mouse PT increased gradually over the 5 days following the transition from the short- to the long-day condition (Figure 2A). Because the PT circadian clock was entrained to the lights-off timing (Figure 1B), we speculated that the observed slow dynamics of *TSH*β induction in the mouse PT were due to the gradual entrainment of the PT circadian clock. We also hypothesized that the "photoinducible" phase (the circadian time when light stimulation can induce *TSH*β expression) is in the subjective (circadian) late night (as defined in the short-day condition), and therefore entrainment over 5 days might be required for full transition of the photoinducible phase to the photoperiod under the long day.

*Correspondence: shigey@med.kindai.ac.jp (Y.S.), uedah-tky@umin.ac.jp (H.R.U.)

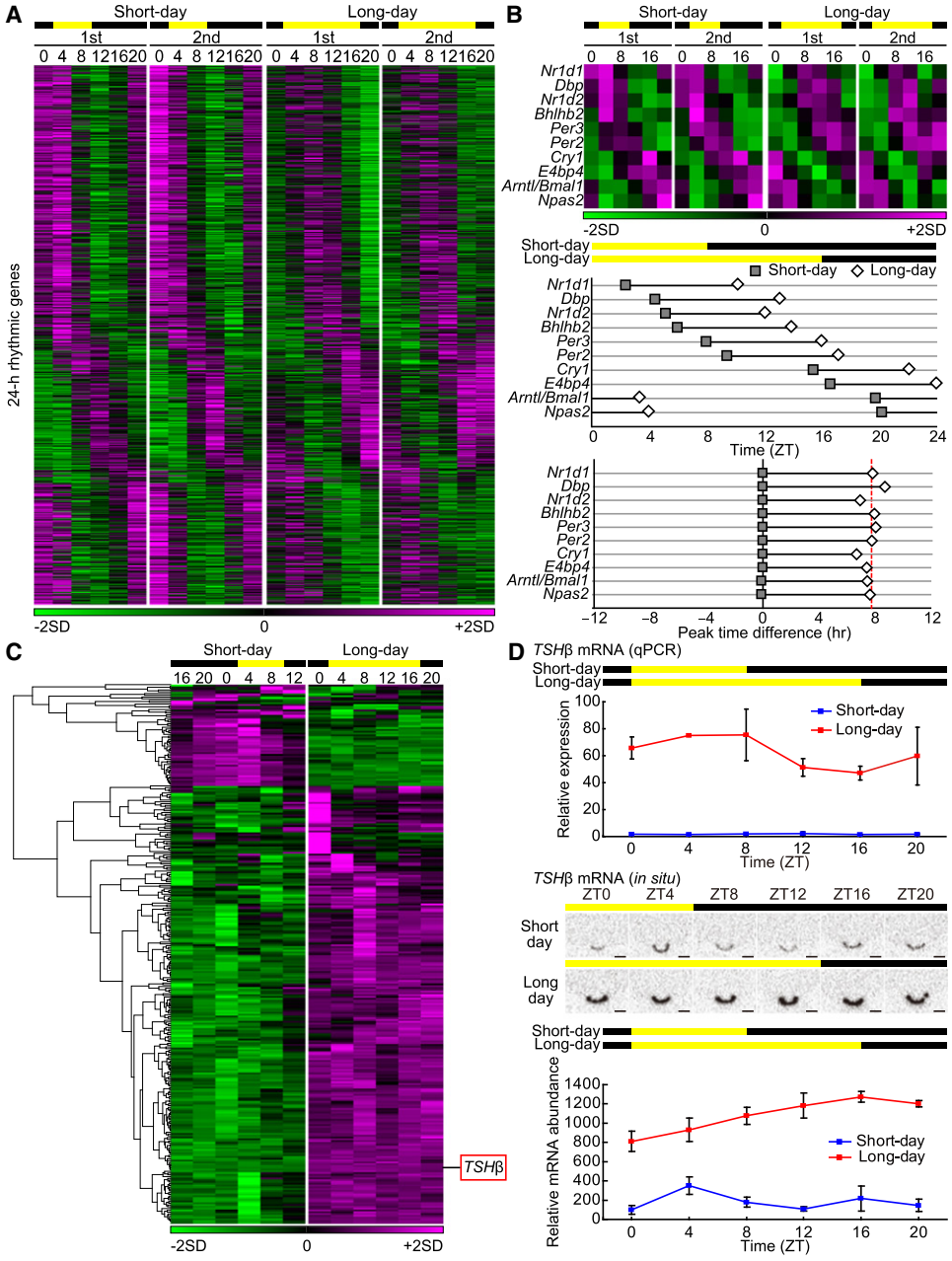

Figure 1. Genome-wide Expression Analysis of Circadian and Photoperiodic Genes in the Mouse Pars Tuberalis under Chronic Short-Day and Long-Day Conditions

(A) Heat map of 24 hr rhythmic genes in the mouse pars tuberalis (PT) under short-day (left two panels) and long-day (right two panels) conditions. In both conditions, time-series data of the first and second experimental replicates are plotted. In the heat maps in (A)–(C), magenta tiles indicate higher gene expression; green tiles indicate lower expression.

(B) Peak-time difference in the circadian expression of clock and clock-controlled genes between short-day and long-day conditions. The upper panel shows a heat map of the clock and clock-controlled genes. The middle panel shows their peak times. The lower panel indicates the difference in peak time between the short-day and long-day conditions. The peak time in the short-day condition for each gene was set to 0. The average difference in peak time was 7.71 hr (dashed red line).

(C) Heat map of photoperiodic genes for which the expression level changed between the short-day and long-day conditions. The location of *TSH*β is indicated.

(D) Confirmation of the GeneChip data for *TSH*β expression. *TSH*β expression under short-day and long-day conditions was measured by qPCR (n = 2, top panels; *TSH*β expression relative to *Tbp* expression is plotted) and radioisotope (RI) in situ hybridization (n = 3, middle and bottom panels; scale bars represent 300 μm). Error bars represent ± standard error of the mean (SEM).

To confirm that the PT circadian clock was gradually shifted in this condition, we used a molecular timetable method [18, 19], which can measure circadian phase from the expression pattern of clock and clock-controlled genes with a single-time-point sample (Supplemental Experimental Procedures). We found that the PT circadian time was

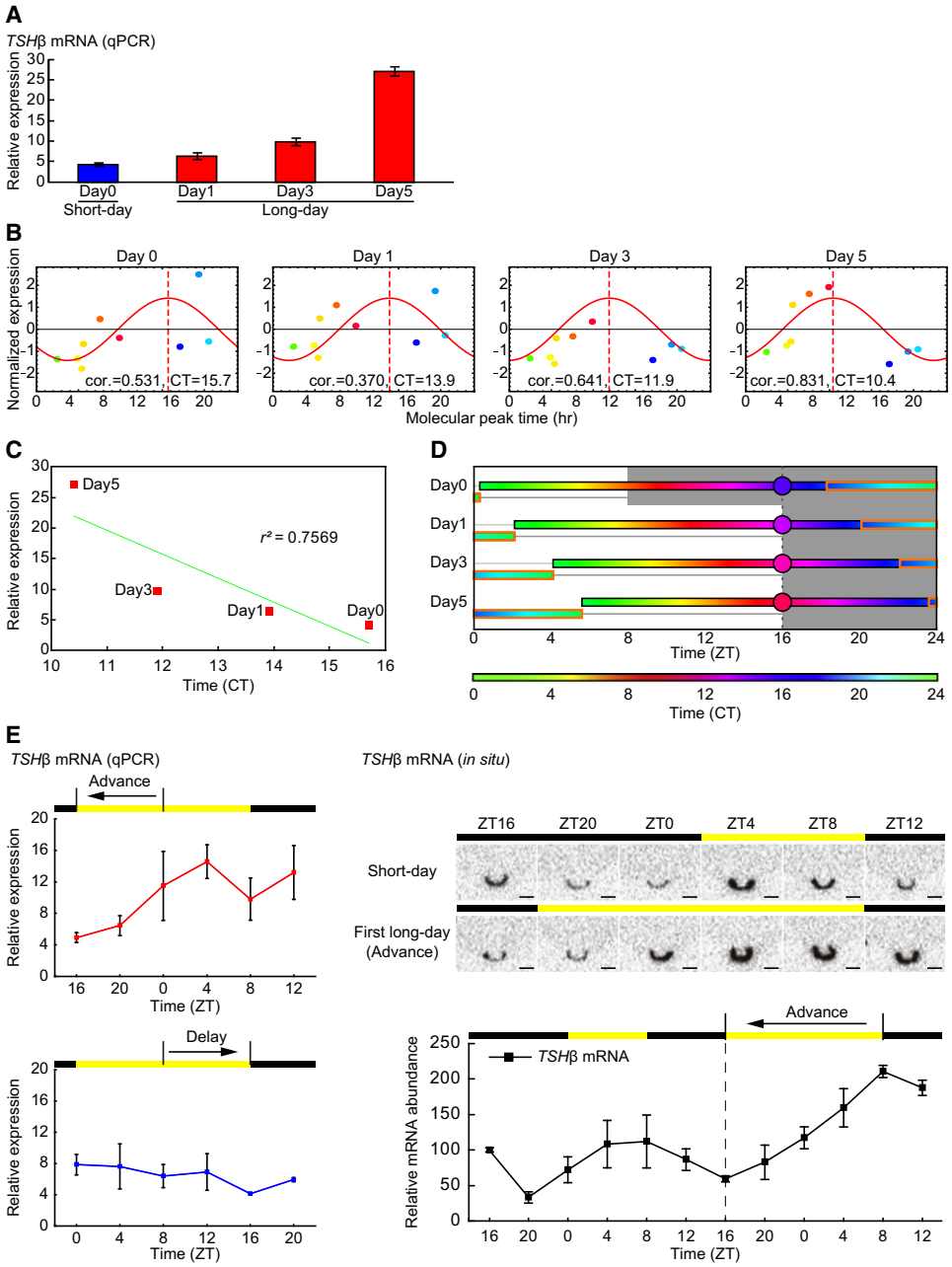

Figure 2. Late-Night Light Stimulation Immediately Induces *TSH*β Expression in the Mouse PT

(A) *TSH*β expression at ZT16 on days 0, 1, 3, and 5 after the transition of light condition, in which lights-off timing was delayed by 8 hr. *TSH*β expression was measured by qPCR (n = 2). *TSH*β expression relative to *Tbp* expression is plotted. Error bars represent ± SEM.

(B) Circadian time measurement from the mouse PT. Colors and x values of the dots indicate the molecular peak time of individual clock and clock-controlled genes. The peak time of the red cosine curve indicates the estimated circadian time (CT, dashed vertical line). The correlation coefficient (cor.) between the red cosine curve and normalized expression data is also indicated in the panel.

(C) Linear regression analysis between the estimated circadian time (CT, x axis) of the PT and quantity of *TSH*β expression (y axis). Red dots indicate data points. Green line indicates regression line. $r^2 = 0.7569$.

(D) Gradual change in the estimated circadian time of the PT from day 0 to day 5. Color bars indicate the estimated circadian time (CT) of the PT on each day. The x axis indicates the environmental zeitgeber time (ZT). The circadian time at ZT16 is indicated by a colored circle. The orange-outlined box indicates the putative photoinducible phase. The background indicates the light conditions (white, light phase; gray, dark phase).

(E) CBA/N mice kept in the short-day condition (light:dark = 8:16 hr) for 3 weeks were then transferred to a long-day condition, in which the dark period was advanced (advance condition) or delayed (delay condition) by 8 hr. Left panels: *TSH*β expression on the first long day (advance and delay conditions) was measured by qPCR (n = 2). *TSH*β expression relative to *Tbp* expression is plotted. Right panels: *TSH*β expression in the short-day condition and on the first long day (advance condition) was measured by RI in situ hybridization (n = 3). Scale bars represent 300 μm. Error bars represent ± SEM.

gradually shifted over 5 days (Figure 2B). We also noted that the circadian time in the PT correlated well with the induction of *TSH*β expression (Figure 2C; $r^2 = 0.7569$), consistent with the hypothesis. Based on these findings, we plotted the measured circadian time and the hypothesized photoinducible phase (i.e., the circadian late-night period) over the 5 days after the shift and superimposed it on the photoperiod (Figure 2D). This plot showed that *TSH*β expression was not induced on the first day as a result of the mismatch between the hypothetical photoinducible phase of the PT (Figure 2D, orange-outlined box) and the photoperiod (Figure 2D, day 1), whereas *TSH*β expression was strongly induced on the fifth day because of the match between the hypothetical photoinducible phase and the photoperiod, after gradual entrainment of the PT over 5 days (Figure 2D, day 5). This result supports our hypothesis that the photoinducible phase is in the circadian late-night period.

Furthermore, this hypothesis also predicted that *TSH*β expression would be strongly induced on the first day in an alternative long-day condition in which the lights-on timing was advanced by 8 hr (hereafter, the "advance" condition). To verify this prediction, we examined *TSH*β expression in the PT under the advance condition, and we found that it increased immediately (Figure 2E; Figure S1D). RI in situ hybridization also confirmed this immediate *TSH*β expression (Figure 2E, right panels). On the other hand, *TSH*β expression was not induced in the delay condition (Figure 2E, left-bottom panel; Figure S1D). These findings suggest that the mouse PT has a photoinducible phase during subjective late night and that light stimulation occurring in the late night can induce *TSH*β expression immediately, i.e., within one day.

Genome-wide Expression Analysis of Acute Long-Day Genes in the Mouse PT

Given the rapid induction of *TSH*β, we reasoned that a genome-wide expression analysis in the advance and delay conditions might allow us to identify the the upstream inductive mechanism of the *TSH*β pathway. Therefore, we performed a second set of genome-wide expression analyses under these acute long-day conditions (Experimental Procedures). The data obtained were then analyzed to extract "acute long-day" genes expressed in the PT (Supplemental Experimental Procedures). This expression analysis identified 34 acute long-day genes in the PT (Figure 3A; Table S4), which included several transcription factors; *Eya3*, *Ror*β, *Maff*, *Crem*, and *Hdac4* (Figure S1D). We focused on *Eya3* as a putative upstream activator of *TSH*β expression because *Crem* and *Hdac4* encode transcriptional repressors [20, 21] and because *Ror*β and *Maff* could not activate the 7.7 kbp promoter of *TSH*β (Figures S2A and S2B). We first confirmed the acute induction of *Eya3* expression in the PT under the advance condition via qPCR and RI in situ hybridization (Figure 3B; Supplemental Results and Discussion).

Eya3 and *Six1* Synergistically Induce *TSH*β Expression

Eya3 is one of four mammalian homologs (*Eya1–4*) of *eya* [22, 23], a transcriptional coactivator involved in fly eye development [24, 25]. *Eya* family members form a complex with a DNA-binding factor of the *Six* family and a corepressor of the *Dach* family. *Six-Eya-Dach* genetic interactions are reported to regulate the transcriptional activation and repression of target genes. Of the *Eya*, *Six*, and *Dach* families, we found that the *Eya3* and *Six1* mRNAs were highly expressed in the PT under the long-day condition whereas the others were weakly or barely expressed (Figure 4A). We therefore examined whether *Eya3* and *Six1* activate the *TSH*β promoter. The transient transfection of *Eya3* or *Six1* increased the *TSH*β promoter activity only slightly, whereas their cotransfection synergistically increased its activation (Figure 4B). In contrast, *Eya3* and *Six1* did not activate the SV40 promoter. We also found that shorter versions of the *TSH*β promoter (Figure 4C) were also synergistically activated by *Eya3* and *Six1* (Figure 4B). We thus used the shortest version of the *TSH*β promoter (0.1 kbp) in the following experiments unless otherwise indicated. We also confirmed that *Eya3* increased *TSH*β promoter activity in a dose-dependent manner when it was expressed alone or with *Six1* (Figure 4D; Figure S2C; Supplemental Results and Discussion).

An So Site Is Important for *Eya3-Six1*-Dependent Activation of the *TSH*β Promoter

It has been reported that *Six* and *Eya* can activate their target genes through different consensus sequences for *Six* binding (MEF3 site, see [26, 27]; So site, see [27–29]). Therefore, we searched for Six consensus sequences in the 0.1 kbp *TSH*β promoter and found one MEF3 site (+1) and two So sites (−45 and −52) upstream of the transcription start site (TSS). These MEF3 and So sites in the *TSH*β promoter are highly conserved among vertebrates (Figure 4C). We first deleted and mutated the one MEF3 site in the *TSH*β promoter and found that it was dispensable for the *Eya3-Six*-dependent activation of the *TSH*β promoter (Figure 4E). We then sequentially deleted the two So sites (Figure 4C, So1 and So2). Although deletion of the So2 site did not affect the *Eya3-Six*-dependent activation of the *TSH*β promoter, deletion of the So1 site significantly decreased the change elicited by the *Eya3-Six*-dependent activation (Figure 4F). These results indicate that the So1 site is essential for the full activation of the *TSH*β promoter by the *Eya3-Six1* complex.

Because *Tef* can increase *TSH*β promoter activity [30], we also examined the contribution of *Tef* and its family member *Hlf* to the 0.1 kbp *TSH*β promoter. We found that *Tef* or *Hlf* synergistically increased the luciferase activity of the *TSH*β promoter when cotransfected with *Eya3* and *Six1* (Figures S2D–S2J; see details in Supplemental Results and Discussion).

Photoinducible Phase at Subjective Late Night

In this study, genome-wide expression analyses of the mouse PT revealed that *TSH*β and *Eya3* expression are induced by late-night light stimulation. Because these expression data might include potentially important factors besides *Eya3* and *TSH*β, we have made them publicly available (http://photoperiodism.brainstars.org/). We further demonstrated that *Eya3* and its partner *Six1* are expressed in the mouse PT and synergistically activate *TSH*β expression through an So site in the *TSH*β promoter. This activation is further enhanced by *Tef* and *Hlf* through a D box close to the So site. Because previous reports described *Eya3* induction in the PT under long-day conditions in birds [4, 5] and sheep [17], its induction under long-day conditions appears to be an evolutionarily conserved molecular mechanism in the photoperiodism of vertebrates. Among the remaining challenges is the in vivo functional analysis of *Eya3*-dependent induction of *TSH*β expression.

Based on these and previous findings, we propose the following hypothetical model for a gradual transition over months from short-day to long-day conditions in the natural environment. As the photoperiod is gradually extended to

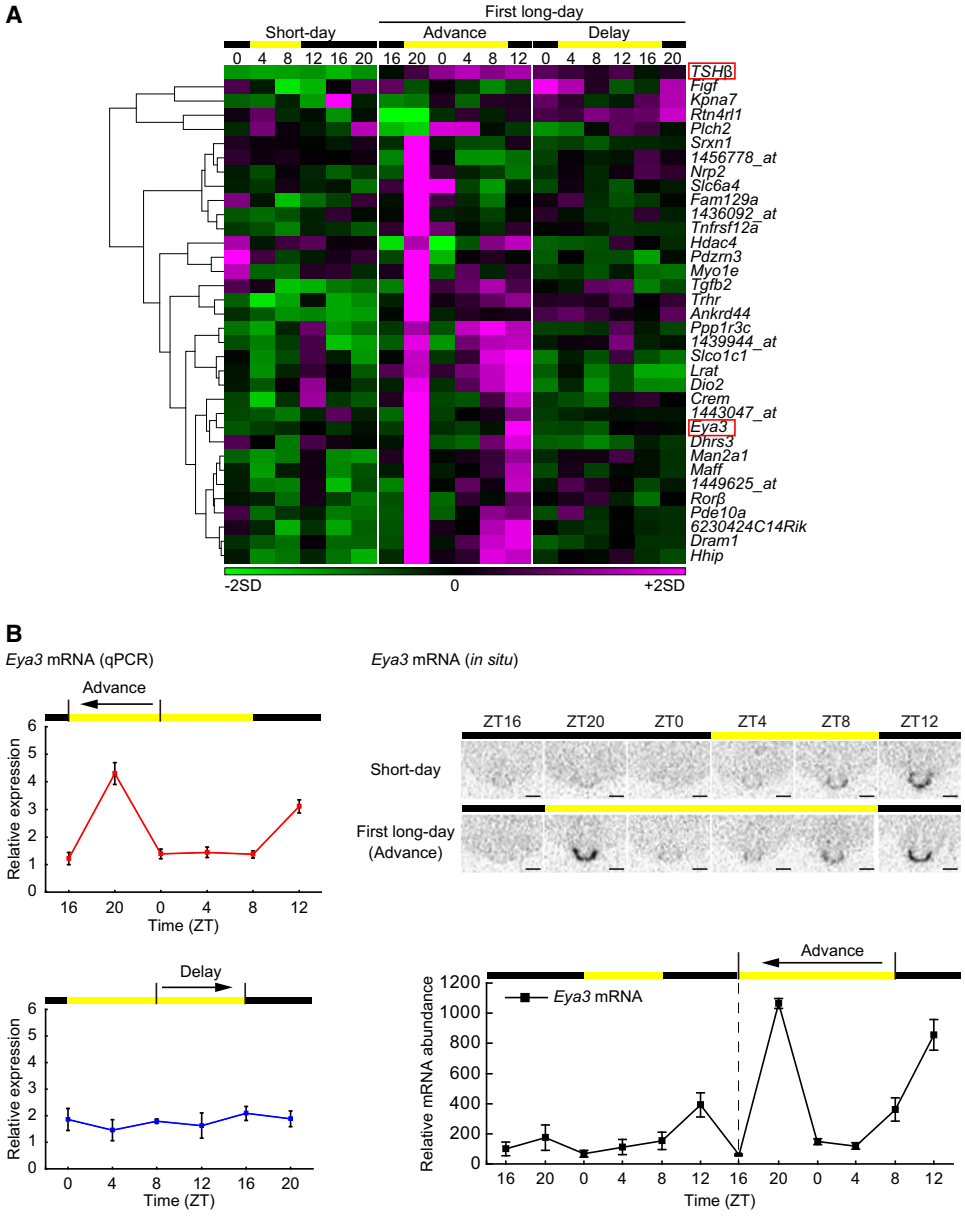

Figure 3. Genome-wide Expression Analysis of Acute Long-Day Genes in the Mouse PT

(A) Heat map of photoperiodic genes whose expression was altered by the photoperiod change only in the advance condition. Magenta tiles indicate higher gene expression in the PT; green tiles indicate lower expression. GeneChip data for *TSH*β expression are displayed for reference.

(B) Confirmation of the GeneChip data for *Eya3* expression. Left panels: *Eya3* expression on the first long day (advance and delay conditions) was measured by qPCR (n = 2). *Eya3* expression relative to *Tbp* expression is plotted. Right panels: *Eya3* expression under the short-day condition and on the first long day (advance condition) was measured by RI in situ hybridization (n = 3). Scale bar represents 300 μm. Error bars represent ± SEM.

completely cover the photoinducible phase (the subjective late night, determined in the short-day condition), *Eya3* is gradually induced, which triggers *TSH*β expression in the PT under natural conditions. These natural and relatively slow expression dynamics can be speeded up by artificial light stimulation at subjective late night, which acutely induces *Eya3* expression. This artificial situation reveals that the mammalian photoperiodic system has unexpectedly rapid dynamics and indicates that the PT of CBA/N mice is an ideal model system for elucidating the remaining molecular mechanisms of photoperiodism (Supplemental Results and Discussion). Identifying the upstream inducer of the acute *Eya3* elevation as well as elucidating the signal transduction cascade from the melatonin receptor to *Eya3* expression will provide further insights into photoperiodism.

Experimental Procedures

Animals and Housing

Male CBA/N mice (Japan SLC, Shizuoka, Japan), which have normal retinas (Supplemental Results and Discussion), were purchased 3 weeks after birth. For chronic long-day and short-day experiments, mice were first housed under short-day conditions (light:dark = 8:16 hr, ZT0 = lights-on, ZT8 = lights-off, 400 lux), given food and water ad libitum, and maintained under these short-day conditions for 3 weeks. The mice were then separated

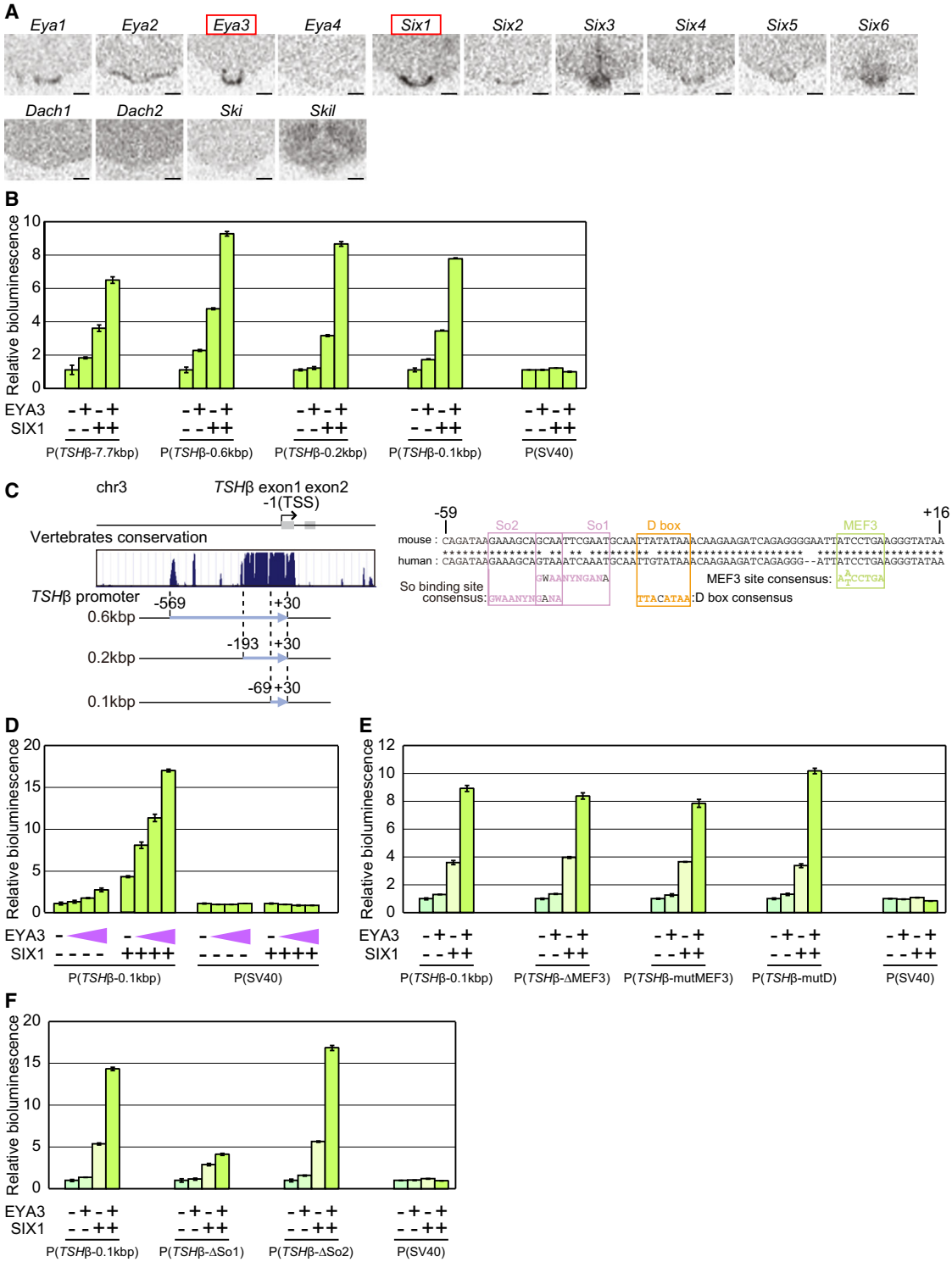

Figure 4. *Eya3* and *Six1* Synergistically Induce *TSH*β Expression

(A) Expression of the *Eya*, *Six*, and *Dach* families in the mouse PT at ZT8 in the long-day condition was detected by RI in situ hybridization. Scale bar represent 300 μm.

(B) The *TSH*β promoter (−7.7 kbp, −0.6 kbp, −0.2 kbp, and −0.1 kbp) is activated by EYA3 and SIX1.

(C) Left: evolutionary conservation scores among vertebrate species were obtained from the UCSC Genome Browser (http://genome.ucsc.edu/). Genomic positions relative to the transcription start site (TSS, also designated as "−1") of the 0.6 kbp, 0.2 kbp, and 0.1 kbp *TSH*β promoter constructs are indicated. Right: the MEF3 site, D box, and So sites in the 0.1 kbp *TSH*β promoter are indicated. Colored letters indicate nucleotides matching the consensus sequence of the MEF3 site, D box, and So sites.

(D) The *TSH*β promoter (−0.1 kbp) is activated by EYA3 in a dose-dependent manner with or without SIX1 (Supplemental Experimental Procedures).

(E) The *TSH*β promoter (−0.1 kbp) and its MEF3-deleted [P(*TSH*β-ΔMEF3)], MEF3-mutated [P(*TSH*β-mutMEF3)], and D box-mutated [P(*TSH*β-mutD)] forms are activated by EYA3 and SIX1.

into two groups. One group was maintained under the short-day conditions and the other was housed under long-day conditions (light:dark = 16:8 hr, ZT0 = lights-on, ZT16 = lights-off, 400 lux) for 2 weeks. Mice in both groups were sacrificed and their PTs were sampled every 4 hr for 1 day, starting at ZT0.

For the acute long-day experiments, mice were first housed under short-day conditions for 3 weeks as described above and then separated into two groups. In one, the lights-on timing was advanced by 8 hr (advance condition), and in the other, the lights-off timing was delayed by 8 hr (delay condition). In both cases, photoperiod was extended by 8 hr. PTs from both groups were obtained every 4 hr for 1 day, starting at the lights-on time (ZT16 in the advance condition and ZT0 in the delay condition, when ZT was defined in the short-day condition).

This study was performed in compliance with the Rules and Regulations of the Animal Care and Use Committee, Kinki University School of Medicine, and carefully followed the Guide for the Care and Use of Laboratory Animals, Kinki University School of Medicine. Mice were also carefully kept and handled according to the RIKEN Regulations for Animal Experiments.

Sampling of PT

Slices (0.5 mm thick) of the brain of CBA/N mice were cut on a mouse brain matrix (Neuroscience, Inc., Tokyo) and frozen, and the PT was punched out with a microdissecting needle (gauge 0.5 mm) under a stereomicroscope. The samples included a small amount of the surrounding tissue, such as the median eminence and ependymal cells. We sampled 25 mice at each time point. This entire procedure was repeated twice (n = 2) to obtain experimental replicates.

Microarray Analysis

Total RNA was prepared from the pooled PT samples obtained at each time point under each condition using TRIzol reagent (GIBCO). cDNA synthesis and cRNA labeling reactions were performed as described previously [31]. Affymetrix high-density oligonucleotide arrays for *Mus musculus* (GeneChip Mouse Genome 430 2.0) were hybridized, stained, and washed according to the Expression Analysis Technical Manual (Affymetrix). The expression values were summarized by the robust multiarray analysis method [32]. The microarray data are available at the NCBI Gene Expression Omnibus (GSE24775) or at our website (http://photoperiodism.brainstars.org/).

Accession Numbers

Microarray data reported herein have been deposited in the NCBI Gene Expression Omnibus with the accession number GSE24775.

Supplemental Information

Supplemental Information includes Supplemental Results and Discussion, two figures, four tables, and Supplemental Experimental Procedures and can be found with this article online at doi:10.1016/j.cub.2010.11.038.

Acknowledgments

We thank Joseph Takahashi for *mPer2*^{Luc} mice and Yoichi Minami and Masayuki Iigo for helpful discussions. We also thank Junko Sakai and Yoko Sakakida for technical assistance. Some calculations were performed by the RIKEN Super Combined Cluster. This work was performed as a part of the Genome Network Project of the Ministry of Education, Culture, Sports, Science and Technology of Japan (H.R.U.). This research was supported by an intramural Grant-in-Aid from the RIKEN Center for Developmental Biology (H.R.U.), the RIKEN President's Fund (H.R.U.), and a Grant-in-Aid for Scientific Research (C) from the Ministry of Education, Culture, Sports, Science and Technology of Japan (Y.S.).

Received: October 17, 2010
Revised: November 10, 2010
Accepted: November 12, 2010
Published online: December 2, 2010

References

1. Dawson, A., King, V.M., Bentley, G.E., and Ball, G.F. (2001). Photoperiodic control of seasonality in birds. J. Biol. Rhythms *16*, 365–380.
2. Ebling, F.J., and Barrett, P. (2008). The regulation of seasonal changes in food intake and body weight. J. Neuroendocrinol. *20*, 827–833.
3. Revel, F.G., Masson-Pévet, M., Pévet, P., Mikkelsen, J.D., and Simonneaux, V. (2009). Melatonin controls seasonal breeding by a network of hypothalamic targets. Neuroendocrinology *90*, 1–14.
4. Nakao, N., Ono, H., Yamamura, T., Anraku, T., Takagi, T., Higashi, K., Yasuo, S., Katou, Y., Kageyama, S., Uno, Y., et al. (2008). Thyrotrophin in the pars tuberalis triggers photoperiodic response. Nature *452*, 317–322.
5. Nakao, N., Ono, H., and Yoshimura, T. (2008). Thyroid hormones and seasonal reproductive neuroendocrine interactions. Reproduction *136*, 1–8.
6. Ono, H., Hoshino, Y., Yasuo, S., Watanabe, M., Nakane, Y., Murai, A., Ebihara, S., Korf, H.W., and Yoshimura, T. (2008). Involvement of thyrotropin in photoperiodic signal transduction in mice. Proc. Natl. Acad. Sci. USA *105*, 18238–18242.
7. Reiter, R.J. (1993). The melatonin rhythm: Both a clock and a calendar. Experientia *49*, 654–664.
8. Lincoln, G.A., Andersson, H., and Loudon, A. (2003). Clock genes in calendar cells as the basis of annual timekeeping in mammals—a unifying hypothesis. J. Endocrinol. *179*, 1–13.
9. Ikegami, K., Katou, Y., Higashi, K., and Yoshimura, T. (2009). Localization of circadian clock protein BMAL1 in the photoperiodic signal transduction machinery in Japanese quail. J. Comp. Neurol. *517*, 397–404.
10. Hoffman, R.A., and Reiter, R.J. (1965). Pineal gland: Influence on gonads of male hamsters. Science *148*, 1609–1611.
11. Bittman, E.L., Karsch, F.J., and Hopkins, J.W. (1983). Role of the pineal gland in ovine photoperiodism: Regulation of seasonal breeding and negative feedback effects of estradiol upon luteinizing hormone secretion. Endocrinology *113*, 329–336.
12. Morgan, P.J., and Williams, L.M. (1996). The pars tuberalis of the pituitary: A gateway for neuroendocrine output. Rev. Reprod. *1*, 153–161.
13. Goldman, B.D. (2001). Mammalian photoperiodic system: Formal properties and neuroendocrine mechanisms of photoperiodic time measurement. J. Biol. Rhythms *16*, 283–301.
14. Hazlerigg, D., and Loudon, A. (2008). New insights into ancient seasonal life timers. Curr. Biol. *18*, R795–R804.
15. Klosen, P., Bienvenu, C., Demarteau, O., Dardente, H., Guerrero, H., Pévet, P., and Masson-Pévet, M. (2002). The mt1 melatonin receptor and RORbeta receptor are co-localized in specific TSH-immunoreactive cells in the pars tuberalis of the rat pituitary. J. Histochem. Cytochem. *50*, 1647–1657.
16. Guilding, C., Hughes, A.T., Brown, T.M., Namvar, S., and Piggins, H.D. (2009). A riot of rhythms: Neuronal and glial circadian oscillators in the mediobasal hypothalamus. Mol. Brain *2*, 28.
17. Dupré, S.M., Miedzinska, K., Duval, C.V., Yu, L., Goodman, R.L., Lincoln, G.A., Davis, J.R., McNeilly, A.S., Burt, D.D., and Loudon, A.S. (2010). Identification of Eya3 and TAC1 as long-day signals in the sheep pituitary. Curr. Biol. *20*, 829–835.
18. Minami, Y., Kasukawa, T., Kakazu, Y., Iigo, M., Sugimoto, M., Ikeda, S., Yasui, A., van der Horst, G.T., Soga, T., and Ueda, H.R. (2009). Measurement of internal body time by blood metabolomics. Proc. Natl. Acad. Sci. USA *106*, 9890–9895.
19. Ueda, H.R., Chen, W., Minami, Y., Honma, S., Honma, K., Iino, M., and Hashimoto, S. (2004). Molecular-timetable methods for detection of body time and rhythm disorders from single-time-point genome-wide expression profiles. Proc. Natl. Acad. Sci. USA *101*, 11227–11232.
20. Jeong, B.C., Hong, C.Y., Chattopadhyay, S., Park, J.H., Gong, E.Y., Kim, H.J., Chun, S.Y., and Lee, K. (2004). Androgen receptor corepressor-19 kDa (ARR19), a leucine-rich protein that represses the transcriptional activity of androgen receptor through recruitment of histone deacetylase. Mol. Endocrinol. *18*, 13–25.

(F) The *TSH*β promoter (−0.1 kbp) and its So2-deleted form [P(*TSH*β-ΔSo2)] are activated by EYA3 and SIX, whereas its So1-deleted form [P(*TSH*β-ΔSo1)] is not.

In (B) and (D)–(F), each of the indicated promoters was fused to a luciferase reporter gene and used to transiently transfect NIH 3T3 cells. The luciferase activity for each promoter is expressed relative to activity with an empty vector. Data are representative of two independent experiments. Error bars represent ± SEM (n = 3).

21. Gordon, J.W., Pagiatakis, C., Salma, J., Du, M., Andreucci, J.J., Zhao, J., Hou, G., Perry, R.L., Dan, Q., Courtman, D., et al. (2009). Protein kinase A-regulated assembly of a MEF2·HDAC4 repressor complex controls c-Jun expression in vascular smooth muscle cells. J. Biol. Chem. *284*, 19027–19042.
22. Xu, P.X., Woo, I., Her, H., Beier, D.R., and Maas, R.L. (1997). Mouse Eya homologues of the Drosophila eyes absent gene require Pax6 for expression in lens and nasal placode. Development *124*, 219–231.
23. Borsani, G., DeGrandi, A., Ballabio, A., Bulfone, A., Bernard, L., Banfi, S., Gattuso, C., Mariani, M., Dixon, M., Donnai, D., et al. (1999). EYA4, a novel vertebrate gene related to Drosophila eyes absent. Hum. Mol. Genet. *8*, 11–23.
24. Bonini, N.M., Leiserson, W.M., and Benzer, S. (1993). The eyes absent gene: Genetic control of cell survival and differentiation in the developing Drosophila eye. Cell *72*, 379–395.
25. Bonini, N.M., Leiserson, W.M., and Benzer, S. (1998). Multiple roles of the eyes absent gene in Drosophila. Dev. Biol. *196*, 42–57.
26. Spitz, F., Demignon, J., Porteu, A., Kahn, A., Concordet, J.P., Daegelen, D., and Maire, P. (1998). Expression of myogenin during embryogenesis is controlled by Six/sine oculis homeoproteins through a conserved MEF3 binding site. Proc. Natl. Acad. Sci. USA *95*, 14220–14225.
27. Li, X., Oghi, K.A., Zhang, J., Krones, A., Bush, K.T., Glass, C.K., Nigam, S.K., Aggarwal, A.K., Maas, R., Rose, D.W., and Rosenfeld, M.G. (2003). Eya protein phosphatase activity regulates Six1-Dach-Eya transcriptional effects in mammalian organogenesis. Nature *426*, 247–254.
28. Pauli, T., Seimiya, M., Blanco, J., and Gehring, W.J. (2005). Identification of functional sine oculis motifs in the autoregulatory element of its own gene, in the eyeless enhancer and in the signalling gene hedgehog. Development *132*, 2771–2782.
29. Giordani, J., Bajard, L., Demignon, J., Daubas, P., Buckingham, M., and Maire, P. (2007). Six proteins regulate the activation of Myf5 expression in embryonic mouse limbs. Proc. Natl. Acad. Sci. USA *104*, 11310–11315.
30. Drolet, D.W., Scully, K.M., Simmons, D.M., Wegner, M., Chu, K.T., Swanson, L.W., and Rosenfeld, M.G. (1991). TEF, a transcription factor expressed specifically in the anterior pituitary during embryogenesis, defines a new class of leucine zipper proteins. Genes Dev. *5*, 1739–1753.
31. Ueda, H.R., Matsumoto, A., Kawamura, M., Iino, M., Tanimura, T., and Hashimoto, S. (2002). Genome-wide transcriptional orchestration of circadian rhythms in Drosophila. J. Biol. Chem. *277*, 14048–14052.
32. Irizarry, R.A., Bolstad, B.M., Collin, F., Cope, L.M., Hobbs, B., and Speed, T.P. (2003). Summaries of Affymetrix GeneChip probe level data. Nucleic Acids Res. *31*, e15.

Current Biology, Volume *20*

Supplemental Information

Acute Induction of *Eya3* by Late-Night Light Stimulation Triggers *TSH*β Expression in Photoperiodism

Koh-hei Masumoto, Maki Ukai-Tadenuma, Takeya Kasukawa, Mamoru Nagano, Kenichiro D. Uno, Kaori Tsujino, Kazumasa Horikawa, Yasufumi Shigeyoshi, and Hiroki R. Ueda

Supplemental Results and Discussion

Circadian Oscillators in the Mouse PT

To investigate whether PT region contains a circadian oscillator, we examined brain slices of *mPer2*^{Luc} mice [1] containing PT and found that the slice exhibited several circadian oscillations of bioluminescence (Figure S1A). Also, it was reported that PER2::LUC rhythms were detected in the median eminence/pars tuberalis [2]. This result and previously report indicate that the PT contains the circadian oscillator.

Circadian Oscillations of Clock and Clock-Controlled Genes in the Mouse PT

Many known clock and clock-controlled genes exhibited 24 hr rhythmicity in the PT under both short-day and long-day conditions (Figure 1B and Table S2). However, some clock and clock-controlled genes are not in the list of 24 hr rhythmic genes. Therefore, we checked 24 hr rhythmicity of known clock and clock-controlled genes in the short-day and long-day conditions by using stringent criteria for 24 hr rhythmicity (correlations > 0.8 both in short-day and long-day conditions). *Per1*, *Clock* and *Tef* exhibited stringent 24 hr rhythmicity in the short-day condition (correlations > 0.8), but not in the long-day condition (correlations < 0.8). *Cry2* and *Hlf* did not exhibit stringent 24 hr rhythmicity either in the short-day or long-day conditions.

Expression of Photoperiodic Gene Candidates in the Mouse PT

The identified photoperiodic genes included *TSH*β. In contrast to the β subunit of TSH (*TSH*β), its α subunit (*Cga*) did not respond to the photoperiod and was not identified as a photoperiodic gene by our statistical analysis (Figure S1B). Recently, tachykinin precursor 1 (*Tac1*), which encodes the tachykinin peptide hormone family members substance P and neurokinin A, was

identified as a long-day gene in the sheep PT, and *Tac1* has been suggested to regulate prolactin release *in vivo* [3]. However, the *Tac1* gene was not identified as a photoperiodic gene by our statistical analysis (Figure S1B), and this finding was confirmed using quantitative PCR (qPCR) (Figure S1C).

Expression Dynamics of *Eya3* and *TSH*β

The induction of *Eya3* was acute and transitory, whereas *TSH*β expression was gradually induced. We consider that the difference between time-scale of *Eya3* and *TSH*β inductions is likely due to a molecular cascade of transcriptional regulation of *Eya3* followed by that of *TSH*β. In general, a cascade of transcriptional regulation can generate the delay in transcription [4]. Therefore, the observed gradual induction of *TSH*β after the acute induction of *Eya3* could be, at least in part, explained by the cascade of transcriptional regulation.

Activation of *TSH*β Promoter by *Eya3*

In Figure 4B, *Eya3*, which is a transcriptional co-activator and does not directly bind to DNA, appears to activate the *TSH*β promoter when transfected alone. We thus measured *Six1* mRNA expression in NIH3T3 cells by qPCR method and found that *Six1* is expressed in the NIH3T3 cells (Figure S2C). Therefore, we speculate that transfection of *Eya3* alone may be able to slightly increase the activation of *TSH*β promoter through the interaction with endogenous *Six1*.

***Tef* and *Hlf* Enhance the *Eya3*-*Six1*-Dependent Activation of *TSH*β Promoter**

Since thyrotroph embryonic factor (*Tef*) can increase the *TSH*β promoter activity [5], we examined the contribution of *Tef* and its family members, hepatic leukemia factor (*Hlf*) and *Dbp* to 7.7-kbp and 0.1-kbp *TSH*β promoter. These PAR bZIP transcription factors can activate various promoters via the D box consensus sequences [6, 7]. *TSH*β promoter contains at least three functional D boxes upstream of the TSS [5]. We first examined the ability of *Tef, Hlf,* and *Dbp* to trans-activate the 7.7-kbp or 0.1-kbp *TSH*β promoter. We found that the transfection of *Tef, Hlf* or *Dbp* significantly increased the Luciferase activity of the 7.7-kbp or 0.1-kbp *TSH*β promoter (Figure S2D, P(*TSH*β-7.7k) and P(*TSH*β-0.1k)), whereas neither activated the SV40 promoter activity, indicating that the *Tef*-, *Hlf*- or *Dbp*-dependent activation of the *TSH*β promoter was specific (Figure S2D, P(SV40)). Consistent with these results, the 0.1-kbp *TSH*β promoter possesses one of the previously identified D boxes [5], which is highly conserved among vertebrates (Figure 4C).

We note that *Dbp* slightly decrease *Luciferase* activity of the 7.7-kbp *TSH*β promoter in combination with the *Tef* or *Hlf*. This result could be simply explained by the weaker activation of 7.7-kbp *TSH*β promoter by *Dbp* alone than that by *Tef* or *Hlf* (Figure S2D, P(*TSH*β-7.7k)). A

weaker transcriptional activator (e.g. *Dbp*) apparently serves as a transcriptional repressor by partially inhibiting the binding of a stronger transcriptional activator (e.g. *Tef or Hlf*). This hypothesis could be confirmed when we use the 0.1-kbp *TSH*β promoter, to which *Dbp, Tef* or *Hlf* activate almost equally. As predicted, we confirmed that *Dbp* does not decrease *Luciferase* activity of 0.1-kbp *TSH*β promoter even in combination with the *Tef* or *Hlf* (Figure S2D, P(*TSH*β-0.1k)).

In addition to *Tef, Hlf,* and *Dbp*, we also examined *E4bp4 (Nfil3),* which is also rhythmically expressed in the PT (Figure 1B) because *E4bp4* can function as either a trans-repressor or trans-activator of transcription in different cell types and promoter contexts [8, 9]. We found that *E4bp4* exhibited no significant effect on 0.1-kbp *TSH*β promoter activity (Figure S2E).

The temporal expression profiles of *Tef, Hlf,* and *Dbp* under the long-day and short-day conditions showed that *Tef* and *Dbp* exhibited 24 hr rhythmicity under both the long-day and short-day conditions. In contrast, *Hlf* exhibited only slight 24 hr rhythmicity under the short-day condition and a photoperiodic response under the long-day condition (Figure S2F).

We next investigated the spatial expressions of *Tef, Hlf* and *Dbp* genes in the mouse PT under the long-day condition by RI *in situ* hybridization (Figure S2G) and found that the *Tef* and *Hlf* mRNAs were highly expressed whereas the *Dbp* mRNA was expressed only weakly. Based on these findings, we hereafter focused on the contribution of *Tef* and *Hlf* to the *Eya3-Six1*-dependent *TSH*β promoter activity. When co-transfected with *Eya3* and *Six1*, *Tef* or *Hlf* synergistically increased the Luciferase activity of the *TSH*β promoter (Figure S2H, P(*TSH*β-0.1k)). We also confirmed that *Eya3* increased the *TSH*β promoter activity in a dose-dependent manner when it was co-expressed with *Six1* and *Tef* or *Hlf* (Figure S2I, P(*TSH*β-0.1k)).

To determine which cis-element(s) in the *TSH*β promoter (P(*TSH*β-0.1k)) were activated by *Tef* and *Hlf*, we mutated the D box as well as the putative Six consensus sequences in the *TSH*β promoter, and then performed Luciferase transfection assays. We found that the mutation of the D box site in the *TSH*β promoter significantly decreased the change elicited by the *Tef*- or *Hlf*-dependent activation (Figure S2J, P(*TSH*β-mutD)). In contrast, neither the mutation nor deletion of the MEF3 site had much effect on the *Tef*- or *Hlf*-dependent activation of the *TSH*β promoter. We also noted that the mutation of the D box site in the *TSH*β promoter did not affect the change elicited by the *Eya3-Six*-dependent activation (Figure 4E, P(*TSH*β-mutD)).

These results indicate that *Tef* and *Hlf* act additively on only one D box in the 0.1-kbp *TSH*β promoter (Figure S2D and J). Since both *Hlf* and *Tef* act as a transcriptional activator of D box, transfection of both *Hlf* and *Tef* into the cells seems equivalent to the increased concentration of a transcriptional activator of D box (either *Hlf* or *Tef*). A transcriptional

activator at higher concentration can bind to a cis-element with higher probability, which will results in the increased transcriptional activity. This simple hypothetical mechanism will explain why co-transfection of both *Hlf* and *Tef* additively activates *TSH*β promoter containing only one D box.

This D box is located near the transcription start site in the *TSH*β promoter, and looks like and might work as a TATA box. To exclude this possibility, we examined the basal activity of the D box-mutated *TSH*β promoter (P(*TSH*β-mutD)) and compared it with the wild type *TSH*β promoter (P(*TSH*β-0.1k)). In fact, the basal activity of P(*TSH*β-mutD) in Figure 4E was 1.16 ± 0.070-fold (average ± SEM, n = 3) of that of wild type P(*TSH*β-0.1k), suggesting that a TATA-like sequence overlapping with D box in the *TSH*β promoter does not serve as a TATA box.

We next examined the effect of deleting either the So1 or So2 site in the *TSH*β promoter (Figure S2J). Deletion of the So1 site slightly decreased the change elicited by the *Tef*- or *Hlf*-dependent activation (Figure S2J). These results suggested that the D box is important for the activation of the *TSH*β promoter by *Tef* or *Hlf* and that the So1 site also, but slightly, affects the activation of the *TSH*β promoter by *Tef* or *Hlf*. We also note that both the D box and the So1 site are important for the *Eya3-Six1-Tef*- or *Eya3-Six1-Hlf*-dependent activation of the *TSH*β promoter (Figure S2J). Deletion of So2 site increased the activation of *TSH*β promoter by co-transfection with *Eya3*, *Six1* and *Tef*. Therefore, So2 site may play a suppressing role in activation of *TSH*β promoter although it is unknown what molecular mechanism functions.

Since the So1 and D box are close to one another in the *TSH*β promoter, and since specific combinations of neighbouring cis-elements can exhibit qualitatively new properties from those of either element alone [10], we speculate that the Six consensus sequence and D box may constitute a composite promoter and provide combinatorial regulation in the photoperiodic response. Consistent with this hypothesis, transcriptional activators of the Six consensus sequence (*Eya3* and *Six1*) and of the D box (*Tef* and *Hlf*) exhibited synergistic activation of the *TSH*β promoter. In addition, deletion of the Six consensus sequence affected the *Tef*- or *Hlf*-dependent activation of the *TSH*β promoter (Figure S2J). In the mouse PT, the *Tef* and *Hlf* mRNAs exhibited circadian expression, peaking in the subjective morning under the short-day condition (Figure S2F). Therefore, we expect that the late-night light stimulation induces the expression of *Eya3* in the PT with timing that ensures that it is co-expressed with *Tef* or *Hlf* during the subjective morning, to synergistically trigger *TSH*β expression.

CBA/N Mice as a Model System for the Study of Photoperiodism

This study provided the first genome-wide expression analysis of the CBA/N mouse PT. Our findings in this study, together with the previous report [11] by Dr. Yoshimura in Nagoya

University, suggest that a photoperiodic response of *TSH*β and much of the photoperiodic machinery are preserved in the PT of the CBA/N mouse. These studies have revealed the usefulness of CBA/N mouse as a model organism for the molecular study of photoperiodic system.

Retinal Degeneration in CBA Mice

It was reported that CBA/J (*rd/rd*) mice have lower sensitivity to light due to the retinal degeneration, whereas CBA/N (+/+) mice have normal light sensitivity [12, 13]. In this study, we used CBA/N mice (+/+), which have normal retina.

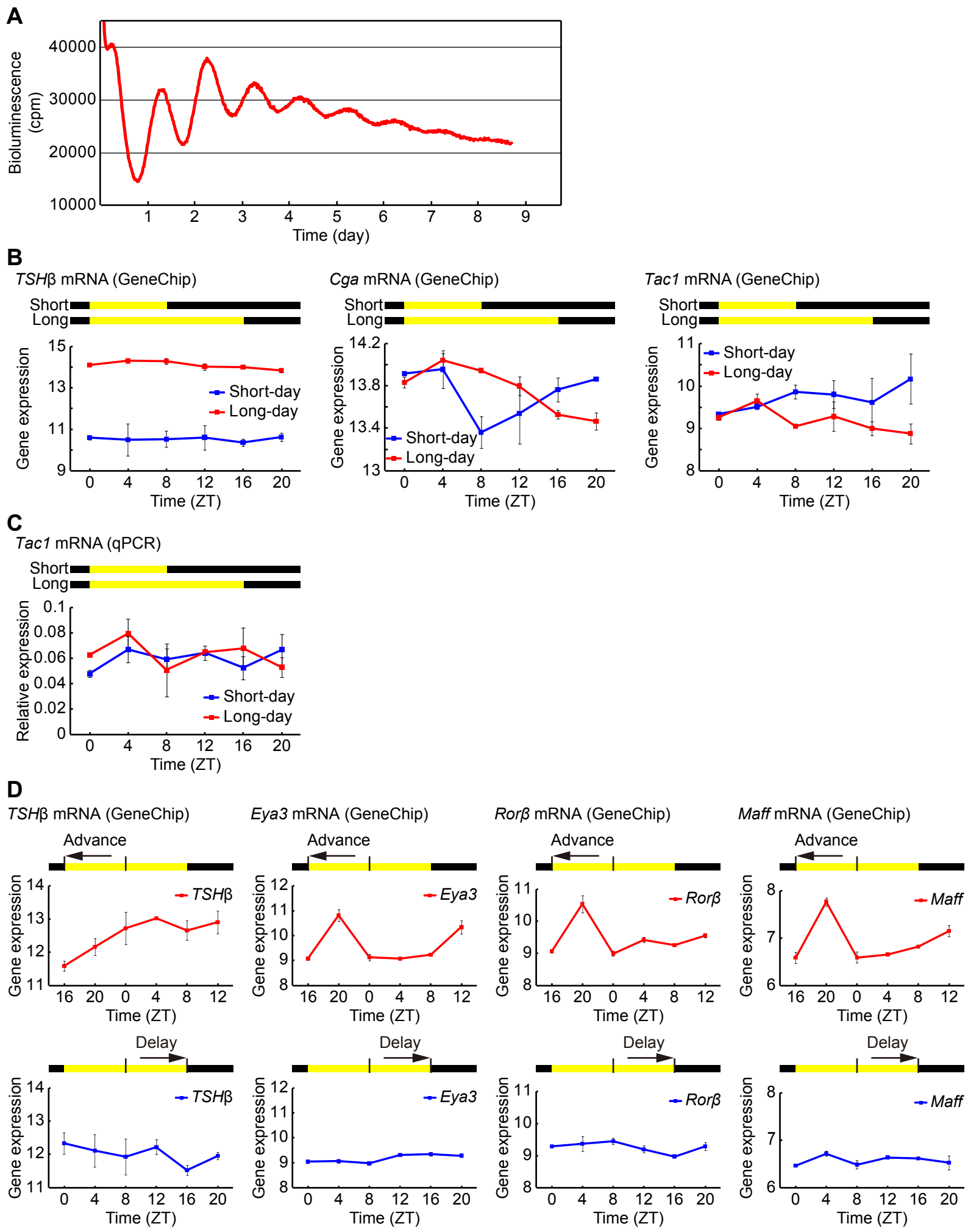

Supplemental Figure 1. Masumoto *et al*.

Figure S1. Expression of Some Photoperiodic and Nonphotoperiodic Genes
(Related to Figure 1)

(A) Representative data of bioluminescence showing circadian profiles of mPER2 expression from PT region from *mPer2*^{Luc} knockin mouse.

(B) Expression of known photoperiodic and nonphotoperiodic genes under the short-day and long-day conditions was measured by GeneChip. The GeneChip data for *TSH*β, *Cga*, and *Tac1* mRNA under the long-day and short-day conditions were indicated by a line plot (n = 2). The vertical axis indicates gene expression on a logarithmic scale (base is 2). Error bars represent ± SEM.

(C) Confirmation of the GeneChip data for the *Tac1* expression. *Tac1* expression under the long-day and short-day conditions measured by qPCR (n = 2). Relative expression to *Tbp* expression is plotted.

(D) GeneChip data of *TSH*β, *Eya3*, *Ror*β, and *Maff* expression on the first long-day (advance and delay conditions) were indicated by a line plot (n = 2). The vertical axis indicates gene expression on a logarithmic scale (base is 2). Error bars represent ± SEM.

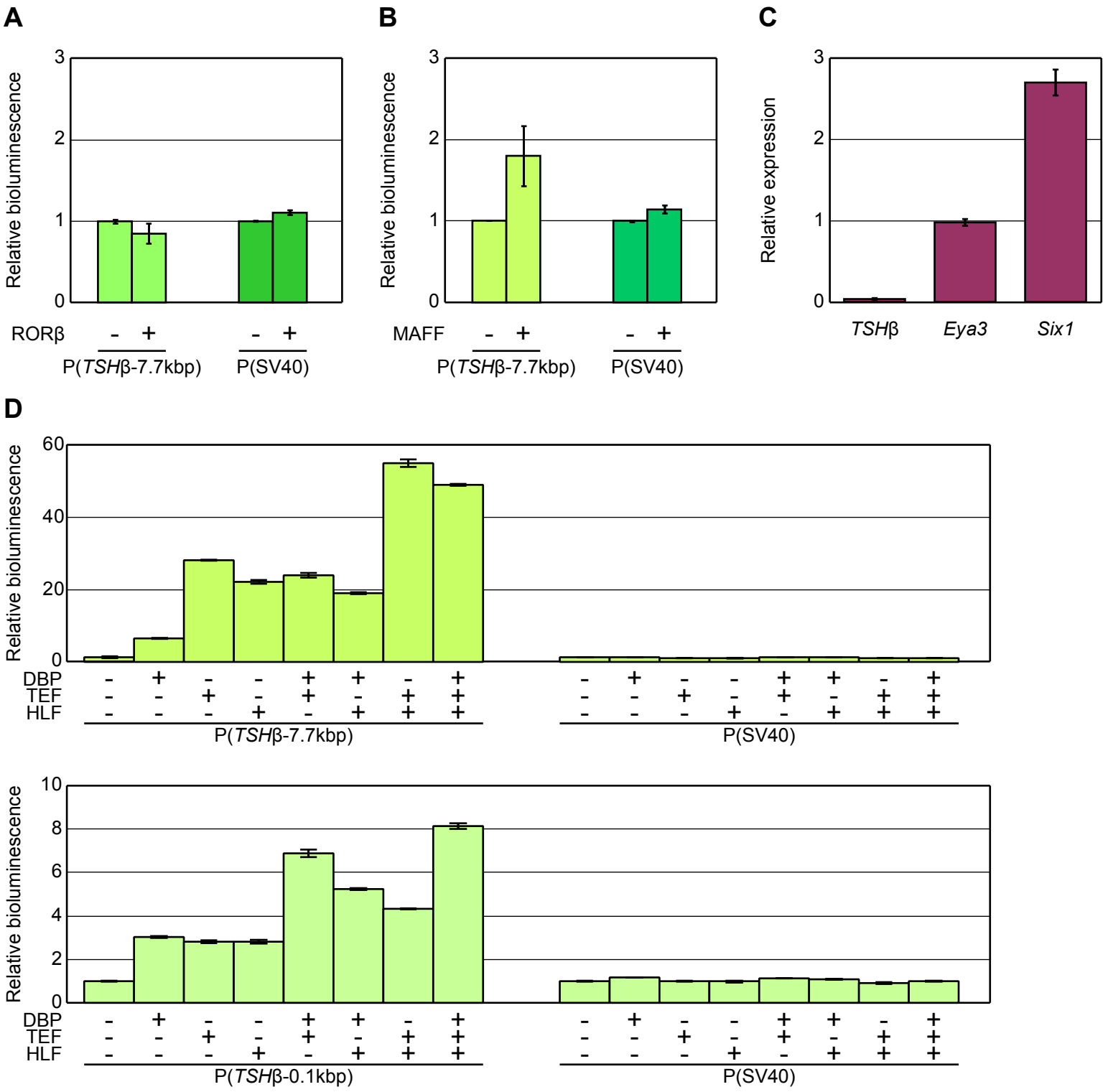

Supplemental Figure 2. Masumoto *et al*. (1/3)

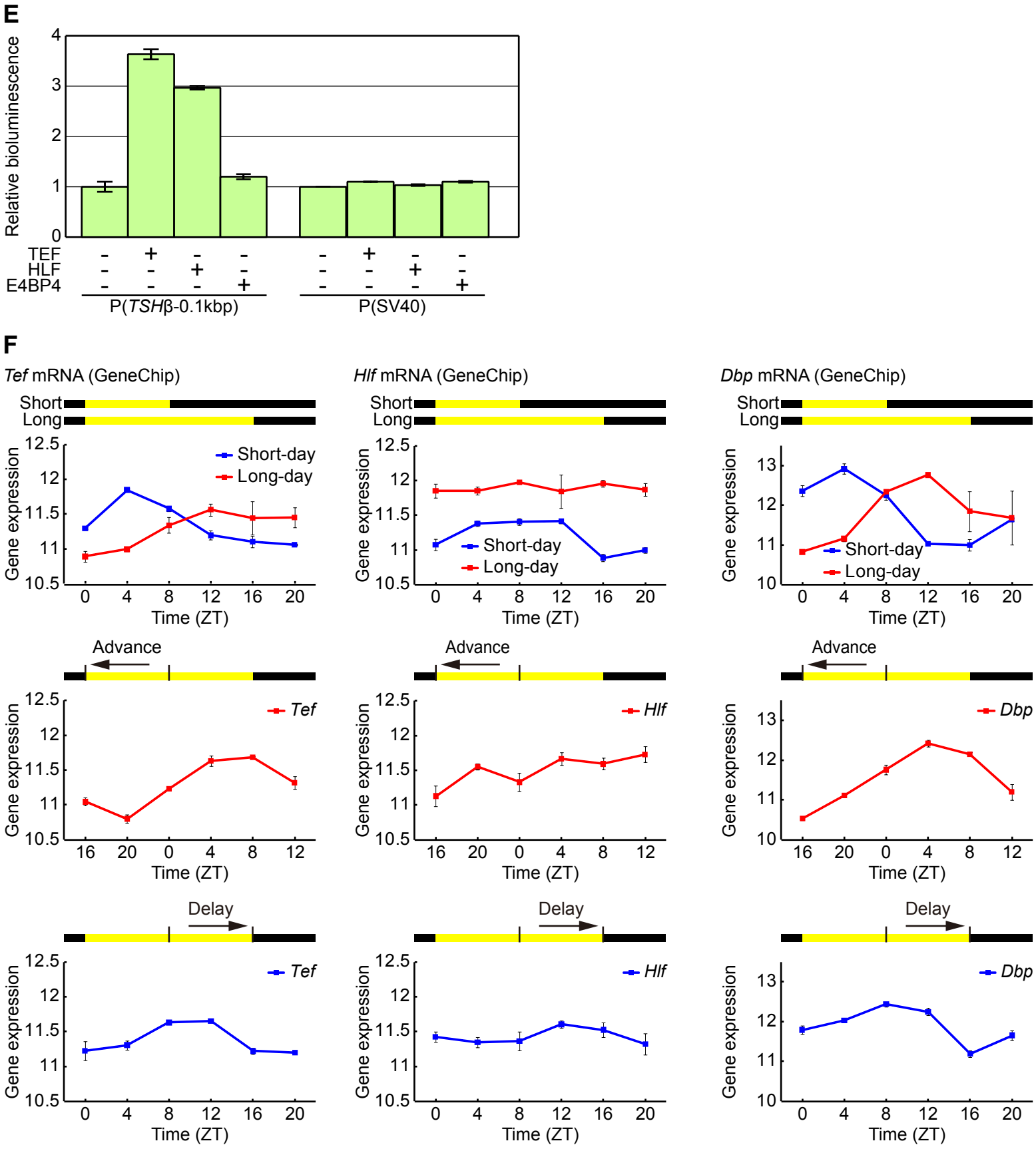

Supplemental Figure 2. Masumoto *et al*. (2/3)

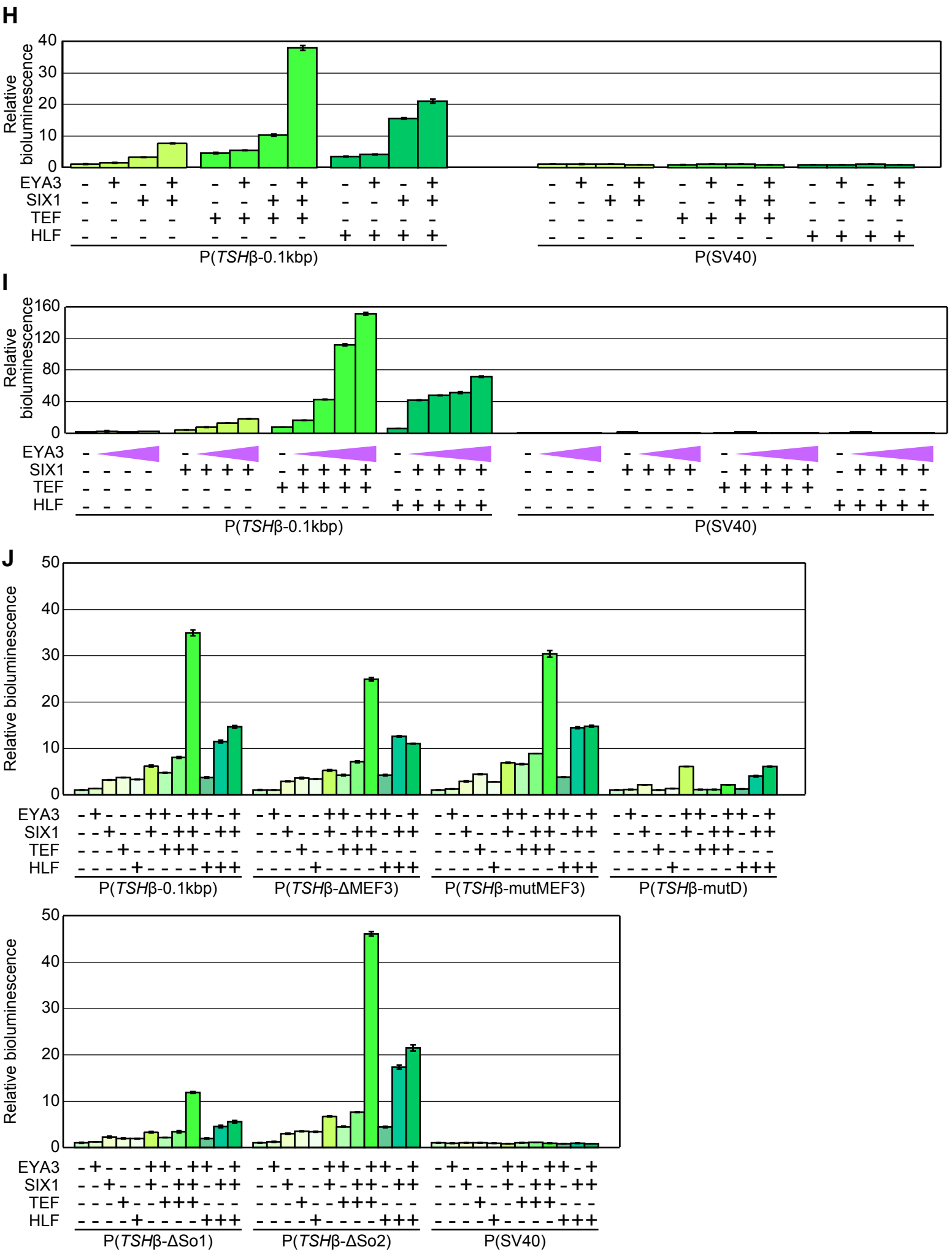

Supplemental Figure 2. Masumoto *et al*. (3/3)

Figure S2. The Activities and the Expression Profiles of the Transcriptional Regulators of the *TSH*β Promoter (Related to Figure 4)

(A and B) RORβ and MAFF had almost no effect on the *TSH*β promoter activity. The *TSH*β promoter (-7.7k) was barely activated by RORβ (A) or MAFF (B).

(C) mRNA expression levels of endogenous *TSH*β, *Eya3* and *Six1* in NIH3T3 cells. Relative mRNA levels of each gene to *Tbp* expression were measured with quantitative PCR assay (n = 3, error bars means ± SEM).

(D) The *TSH*β promoter (-7.7k and -0.1k) could be activated by TEF, HLF, and DBP.

(E) The *TSH*β promoter (-0.1k) was barely activated by E4BP4 (*Nfil3*).

(F) Gene expression of *Tef*, *Hlf*, and *Dbp*. GeneChip data for the *Tef*, *Hlf*, and *Dbp* expression under the short-day and long-day conditions and on the first long-day (advance and delay conditions) indicated by line plot (n = 2). The vertical axis indicates gene expression on a logarithmic scale (base is 2). Error bars means ± SEM.

(G) *Tef*, *Hlf*, and *Dbp* expression in the mouse PT at ZT8 under the long-day condition, detected by RI *in situ* hybridization. Scale bar=300 μm.

(H) *Tef* and *Hlf* enhance the *Eya3*-*Six1*-dependent activation of *TSH*β promoter. The *TSH*β promoter (-0.1k) was strongly activated by EYA3, SIX1, and TEF or HLF. Experiments of Figure 4B and Figure S2H were performed at the same time, so Luciferase activities of P(*TSH*β-0.1k) and P(SV40) in Figure 4B were re-plotted in Figure S2H as control data.

(I) *TSH*β expression is synergistically activated by *Eya3* and *Six1*, and further enhanced by *Tef* and *Hlf*.

(J) Role of the D box and So1 site in transcriptional activation of the *TSH*β promoter by *Eya3*, *Six1*, and *Tef* or *Hlf*. (Top panel) The *TSH*β promoter (-0.1k), and its MEF3-deleted (P(*TSH*β-ΔMEF3)) and MEF3-mutated (P(*TSH*β-mutMEF3)) forms were strongly activated by EYA3, SIX1, and TEF or HLF. The D box-mutated *TSH*β promoter (P(*TSH*β-mutD)) was not activated by TEF and HLF. (Bottom panel) The So2-deleted form (P(*TSH*β-ΔSo2)) were strongly activated by EYA3, SIX1, and TEF or HLF. The So1-deleted *TSH*β promoter (P(*TSH*β-ΔSo1)) was not strongly activated.

(A, B, D, E, H-J) Each of the indicated promoters was fused to a Luciferase reporter gene and used to transiently transfect NIH3T3 cells. The Luciferase activity for each promoter is expressed relative to the activity with an empty vector. Data are representative of two independent experiments. Error bars means ± SEM. (n = 3).

Supplemental Tables (*see accompanying Excel spreadsheet*)

Table S1. List of 24 hr Rhythmic Genes in the Mouse PT under Short-Day and Long-Day Conditions (Related to Figure 1A)

The table provides the Affymetrix probe set ID, p value, FDR, mean of the phases under short-day and long-day conditions, phase difference between short-day and long-day conditions, phase in the short-day condition, phase in the long-day condition, the best Pearson's correlation to cosine curves of a 24 hr period in short-day condition, the best Pearson's correlation to cosine curves of a 24 hr period in long-day condition, amplitude of circadian expression in short-day condition, amplitude in long-day condition, relative amplitude in short-day condition, relative amplitude in long-day condition, p value in short-day condition, p value in long-day condition, description of the probe set, gene name, and gene symbol.

Table S2. List of Clock and Clock-Controlled Genes with Significant Circadian Expression under Short-Day and Long-Day Conditions (Related to Figure 1B)

The table provides the gene symbol, Affymetrix probe set ID, phase in short-day condition, the best Pearson's correlation to cosine curves of a 24 hr period in short-day condition, phase in long-day condition, the best Pearson's correlation to cosine curves of a 24 hr period in long-day condition, the minimum of the values in the 4th and 6th columns (the smaller value of two best Pearson's correlation), and difference between the phases in short-day and long-day conditions.

Table S3. List of Long-Day and Short-Day Genes under Chronic Short-Day and Long-Day Conditions (Related to Figure 1C)

The table provides the Affymetrix probe set ID, p value, FDR, q value, whether the expression in long-day condition is up-regulated ('up') or down-regulated ('down') against the short-day condition, fold change between the mean expression in short-day and long-day conditions, description of the probe set, gene name, and gene symbol.

Table S4. List of Acute Long-Day Genes (Related to Figure 3A)

The table provides the Affymetrix probe set ID, p value, FDR, q value of difference between short-day and advance conditions, maximum fold change between the lowest and highest mean expressions in the short-day and advance conditions, p value, FDR, q value of difference between short-day and delay conditions, maximum fold change between the lowest and highest mean expressions in the short-day and delay conditions, description of the probe set, gene name, and gene symbol.

Supplemental Experimental Procedures

Circadian-Time Analysis from Time-Course Expression Data

To detect how much the circadian phase differed between the short-day and long-day conditions, we investigated the expressions of the following 20 clock and clock-controlled genes by GeneChip: *Bmal1* (*Arntl*), *Bmal2* (*Arntl2*), *Clock*, *Cry1*, *Cry2*, *Dbp*, *Dec1* (*Bhlhb2*), *Dec2* (*Bhlhb3*), *E4bp4* (*Nfil3*), *Npas2*, *Per1*, *Per2*, *Per3*, *Tef*, *Hlf*, *Rev-Erbα* (*Nr1d1*), *Rev-Erb*β (*Nr1d2*), *Rorα*, *Ror*β, and *Rorγ*. We used natural expression values from the GeneChip data. We concatenated two time-courses of experimental replicates (6 time points for each replicate) and used 12 time-point dataset for the subsequent analysis. For each gene, we calculated the best Pearson's correlation between gene expression data and cosine curves of a 24 hr period, and determined its phase in short-day and long-day conditions using a Fourier transformation-based method [14]. If the GeneChip had multiple probe sets for a single gene, we first calculated, for each probe set, two best Pearson's correlation from short-day and long-day conditions, respectively, and then registered the smaller best Pearson's correlation. We selected the probe set with the maximum value of the registered (i.e. smaller) best Pearson's correlation. Next, we chose genes for which the best Pearson's correlation for both the short-day and long-day conditions was more than or equal to 0.8 (see Figure 1B). Finally, we calculated the median of the phase difference (long-day – short-day) for these RNAs. We used this median value (~7.71 hours) as the phase delay of the long-day versus the short-day condition.

Identification of 24 hr Rhythmic Genes

As described above, we concatenated two time-courses of experimental replicates (6 time points for each replicate) and used 12 time-point dataset for the subsequent analysis. To identify 24 hr rhythmic genes in the mouse PT, we first calculated the best Pearson's correlation between gene expression data and cosine curves of a 24 hr period, and determined its phase in short-day and long-day conditions using a Fourier transformation-based method [14]. We then calculated the p values for the best correlations of the short-day and long-day using random shuffling, and then combined these two p values with Fisher's method ($P = P_1 P_2 \{1 - \log(P_1 P_2)\}$). We estimated the false-discovery rates (FDRs) of the combined p value based on the Benjamini-Hochberg method [15], and selected significantly oscillating genes as those for which the FDRs were less than or equal to 0.05.

Identification of Photoperiodic Genes

To identify the photoperiodic genes, we used time-course expression data under chronic short-day and long-day conditions. In order to complement the observed phase difference

between short-day and long-day conditions (the approximately 8 hours, see above), we shifted time points by 8 hours; that is, the short-day ZT16, 20, 0, 4, 8, 12 corresponded to long-day ZT0, 4, 8, 12, 16, 20, respectively. We used log-2-transformed expression values of the GeneChip data in the following analysis. We performed a two-way ANOVA to test the difference in expression levels between the short-day and long-day conditions for each probe set, and assigned p values and FDRs. We selected as significantly differently expressed genes those whose FDRs were less than or equal to 0.05 and for which the difference between the maximum expression value in the short-day condition and the minimum value in the long-day condition ("short-day" gene) or between the maximum expression in the long-day condition and the minimum in the short-day condition ("long-day" gene) was more than 2.5-fold. In this method, we did not subtract the 24 hr rhythmic genes that were identified above, and thus 38 genes were identified both in the 24 hr rhythmic and the photoperiodic genes.

Circadian-Time Estimation from Single-Time-Point Expression Data

To estimate how the circadian phases at ZT16 were changed on days 0, 1, 3 and 5 after transition from the short-day to the delay condition, we used a previously reported molecular-timetable method [16, 17]. To construct a molecular timetable that has the phase (peak time), mean, and standard deviation (SD) of the gene expressions of clock and clock-controlled genes, we used the expression values of 20 clock and clock-controlled genes from the qPCR data at every 4 hours during 48 hours in the short-day condition. We first normalized the qPCR expression data of the 20 clock and clock-controlled genes by using *Tbp* expression level at the same time point. We then calculated the best Pearson's correlation between cosine curves of a 24 hr period and the qPCR expression data. We selected genes with the best Pearson's correlation ≥ 0.8. For these genes, we also calculated peak time, mean and SD of the qPCR expression data. With this molecular timetable, we determined the circadian phase of the mouse PTs at ZT16 on days 0, 1, 3, and 5. In details, we normalized each qPCR expression value obtained at ZT16 for each day by subtracting the estimated mean and then divided by the SD in the molecular timetable. We then plotted the data on a graph, with the phase (peak time) on the x-axis and normalized expression values on the y-axis. From this graph, we searched for the cosine curve, $y = \sqrt{2} \times \mathrm{Cos}(x-b)$, that had the maximum correlation, and determined b as the phase of the day.

Identification of Acute Long-Day Genes

To identify acute long-day genes whose expression patterns were changed on the first long-day after the transition from the short-day to the long-day condition, we sought to retrieve probe sets whose expression patterns in the short-day condition and advance condition were significantly different but whose expression patterns in the short-day condition and delay condition were not

significantly different. First, we estimated that the phase delay of the advance condition and the delay condition against the short-day condition was approximately 0 hours (~0.88 hours), and 4 hours (~3.96 hours), respectively, using the method described in the above circadian-time analysis from the time-course expression data. In order to complement these phase differences, we set the short-day ZT0 to correspond with the advance condition ZT0, and the short-day ZT20 with the delay condition ZT0. We then performed the same statistical procedures described above for identifying genes whose time-course expression patterns in the short-day and long-day condition were different. In this case, we chose genes whose expressions were significantly different between the short-day condition and the advance condition, but were not significant between the short-day condition and the delay condition.

Preparation of PT Region Slices from *mPer2*^{Luc} Mice

The brains were removed from quickly decapitated, young (older than 4 weeks of age) *mPer2*^{Luc} mice, then 300-μm thick coronal sections containing the PT were made using a vibratome type linearslicer (PRO7; Dosaka EM Corp) in ice cold Hanks' balanced salt solution (Invitrogen). PT region slices included a small amount of the surrounding tissue. The slices were then placed on a culture membrane (MilliCell-CM; Millipore) and set on a dish with 1.2 mL culture medium [DMEM supplemented with 1.2 g/L $NaHCO_3$ (Nacalai Tesque), 15 mM HEPES (Dojindo), 20 mg/L kanamycin (Invitrogen), 5 μg/mL insulin (Sigma), 20 nM putrescine (Sigma), 100 μg/mL apo-transferrin (Sigma), 20 nM progesterone (Sigma), 30 nM sodium selenite (Sigma), one-fiftieth part B-27 supplement (Invitrogen), and 1 mM luciferin]. The culture dishes were placed in a high-sensitivity bioluminescence detection system (LM-2400; Hamamatsu Photonics), and the bioluminescence of each well was measured at 37°C.

Quantitative PCR (qPCR) of PT Samples

The total RNA was prepared from the pooled PT samples obtained at each time point under each condition, using Trizol reagent (Gibco BRL). qPCR was performed with the ABI Prism 7900 and SYBR Green Reagents (Applied Biosystems). The cDNAs were synthesized from 0.25 μg of total RNA using Superscript II reverse transcriptase (Invitrogen). Samples contained 1×SYBR Green Master Mix, 0.8 μM primers, and 1/40 synthesized cDNA in a 10 μl volume. The PCR conditions were as follows: 10 min at 95ºC, then 45 cycles of 15 s at 94ºC, 1 min at 59ºC. The absolute cDNA abundance was calculated using a standard curve obtained from murine genomic DNAs. We used *Tbp* as the internal control.

Oligonucleotide Sequences for qPCR of Tissue Samples

The primers (Hokkaido System Science) used in qPCR were as follows:

***TSH*β mRNA:**

Forward primer: 5'-CTGCATACACGAGGCTGTCAG -3'

Reverse primer: 5'-CCCCAGATAGAAAGACTGCGG-3'

***Eya3* mRNA:**

Forward primer: 5'-TTCACAGCTCCAAGTAGAATCTGACT-3'

Reverse primer: 5'-TATGGAAGCGCCATGAGCTT-3'

***Tac1* mRNA:**

Forward primer: 5'-TAATGTGGTGACCTCCCCAGA-3'

Reverse primer: 5'-TCATCACTGTGCTTTGCTGAAA-3'

***Tbp* mRNA:**

Forward primer: 5'-CCCCCTCTGCACTGAAATCA -3'

Reverse primer: 5'-GTAGCAGCACAGAGCAAGCAA -3'

In Situ Hybridization (ISH)

Mice were deeply anesthetized with ether and intracardially perfused with 10 ml saline and 20 ml of a fixative containing 4% paraformaldehyde in 0.1 M phosphate buffer (PB), pH 7.4. Mouse brain samples were postfixed in the same fixative for 24 hours at 4°C, soaked in PB containing 20% sucrose for 48 hours, and stored frozen at -70ºC. The ISH method was described in detail previously [18]. Serial coronal sections (40-μm thick) of the mouse brain were made using a cryostat. Fragments of cDNA were obtained by PCR, and the products were subcloned into the pGEM-T easy vector (Promega). Radiolabelled probes were generated using ^{35}S-UTP (PerkinElmer) via a standard protocol for cRNA synthesis. The probe sequence information is presented in the Supplemental Experimental Procedures.

Oligonucleotide Sequences for ISH

The primers (Hokkaido System Science) used in the construction of ISH cRNA probes were as follows:

***TSH*β cRNA probe:**

Forward primer: 5'-TGGGTGGAGAAGAGTGAGCG-3'

Reverse primer: 5'-ACCAGATTGCACTGCTATTG-3'

***Eya1* cRNA probe:**

Forward primer: 5'-GGACTTTACTACATAACTGGGTCAGCAGC-3'

Reverse primer: 5'-GGTCTCAACACTGGCCATTTCTGTCTG-3'

***Eya2* cRNA probe:**

Forward primer: 5'-GAATCATGCAGAGGTTTGGCCGCAAAG-3'

Reverse primer: 5'-CTCCCTTGCCAATGCCCAGAGAATGATTG-3'

***Eya3* cRNA probe:**

Forward primer: 5'-AGCACAAATGCCAGCCTGATACCCAC-3'

Reverse primer: 5'-CTGTTGGGTCCTTTCCATACTTCTG-3'

***Eya4* cRNA probe:**

Forward primer: 5'-TGCCAACAGGTGTGAGAGGAGGAGTG-3'

Reverse primer: 5'-CCAGTGCTTGATGTAGAGCCAAGAGGTCC-3'

***Six1* cRNA probe:**

Forward primer: 5'-CCTCCTCCTCGTCTTCTTTTAATGAACAGA-3'

Reverse primer: 5'-GAGGCAGCCTACAGATAGGAGAGTTTCTG-3'

***Six2* cRNA probe:**

Forward primer: 5'-CCCCGCTTTACGTTTTCTCTTTCCCTCCT-3'

Reverse primer: 5'-GCAGAAATATCTCCCGACGAACATTCACA-3'

***Six3* cRNA probe:**

Forward primer: 5'-ACATCGAGCGGCTGGGCCGCTTCCTCTG-3'

Reverse primer: 5'-CGATGGCCTGATGCTGGAGCCTGTTCTTG-3'

***Six4* cRNA probe:**

Forward primer: 5'-CGTGATCTCCTTGCACAGAATTGCAAATG-3'

Reverse primer: 5'-CATGCAGAATAACAAGGGTACATACAGAGA-3'

***Six5* cRNA probe:**

Forward primer: 5'-TGACAATGGTGTCAAGGTGCTAGGACAGG-3'

Reverse primer: 5'-GTTGCCCTAGGGAACAGGGAAATCTTTGG-3'

***Six6* cRNA probe:**

Forward primer: 5'-CATCCAGCGACAGTGAGTGCGACATCTG-3'

Reverse primer: 5'-TCACACAGAACGCGTGAGCTTGCTCATTC-3'

***Dach1* cRNA probe:**

Forward primer: 5'-TGGTCATGACATGGGGCATGAGTCAAAAC-3'

Reverse primer: 5'-GGGGTCAGGGAGTCATTTAAGACCCGGAG-3'

***Dach2* cRNA probe:**

Forward primer: 5'-GAGGGATAATAAAGAAGAAGTACCAGCTC-3'

Reverse primer: 5'-CATAGCAGCACTGTCATGCGGCGTTCCAC-3'

***Ski* cRNA probe:**

Forward primer: 5'-CAAATTTCAGAGAAGGGAGGTGAGGTTTC-3'

Reverse primer: 5'-AGGTAGGGTAGGCATGTGGGGAGAAAC-3'

***Skil* cRNA probe:**

Forward primer: 5'-AGATACCTCACTTGAGAATAAAGAAAGCAC-3'

Reverse primer: 5'-GGCATGAAAATGGCAAACATCTCAAAATAC-3'

***Dbp* cRNA probe:**

Forward primer: 5'-ACCGCGCAGGCTTGACATCTAGGGAC-3'

Reverse primer: 5'-CATGACGTTCTTCGGGCACCTAGCTGG-3'

***Tef* cRNA probe:**

Forward primer: 5'-TGGAAAGAGCCACCCTTTGGAGGAC-3'

Reverse primer: 5'-CACACACATGTAAGGCCAAAGGGCTGC-3'

***Hlf* cRNA probe:**

Forward primer: 5'-GTGCATGACCAGAATATTCTCAGGACAGGG-3'

Reverse primer: 5'-CGGAGAAACCACAGTTTGTGACAACACC-3'

qPCR of NIH3T3 Cell Samples

NIH3T3 cells were grown in DMEM (Invitrogen) supplemented with 10% FBS (JRH Biosciences) and antibiotics (100 U/ml penicillin and 100 µg/ml streptomycin; Invitrogen). Total RNA was prepared from NIH3T3 cells using TRIzol reagents (Invitrogen) according to the manufacturer's instructions. The cDNA was synthesized from 0.25 µg of total RNA with random 6 mer (Promega) and Superscript II Reverse Transcriptase (Invitrogen) according to the manufacturer's instructions. qPCR was performed using ABI Prism 7900 and Power SYBR Green Reagents (Applied Biosystems). Samples contained 1×Power SYBR Green Master Mix (Applied Biosystems), 0.8 µM primers and 1/40 synthesized cDNA in a 10 µl volume. PCR conditions were as follows: 10 min at 95ºC, then 45 cycles of 15 s at 94ºC and 1 min at 59ºC. Absolute cDNA abundance was calculated using a standard curve obtained from murine genomic DNA. *Tbp* expression levels were quantified and used as an internal control.

Oligonucleotide Sequences for qPCR

The primers (Hokkaido System Science) used in qPCR were as follows:

***TSH*β mRNA:**

Forward primer: 5'-CTGCATACACGAGGCTGTCAG-3'

Reverse primer: 5'-CCCCAGATAGAAAGACTGCGG-3'

***Eya3* mRNA:**

Forward primer: 5'-TTCACAGCTCCAAGTAGAATCTGACT-3'

Reverse primer: 5'-TATGGAAGCGCCATGAGCTT-3'

***Six1* mRNA:**

Forward primer: 5'-TATTTTTGAAGTCTGTCACCCGAA-3'

Reverse primer: 5'-TTCGTCATATCATTAACCTAGCCACT-3'

***Tbp* mRNA:**

Forward primer: 5'-CCCCCTCTGCACTGAAATCA-3'

Reverse primer: 5'-GTAGCAGCACAGAGCAAGCAA-3'

Transfection and Luciferase Assay

NIH3T3 cells (American Type Culture Collection) were maintained in DMEM (Invitrogen) supplemented with 10% FBS (JRH Biosciences) and antibiotics (100 U/ml penicillin and 100 µg/ml streptomycin; Invitrogen). One day prior to transfection, the cells were plated onto 35-mm dishes at a density of 2×10^5 cells per dish. The following day, the cells were co-transfected using FuGene6 (Roche) with 0.4 µg of a *Luciferase* reporter plasmid in the presence of the following constructs, as indicated in the respective figures: 0 or 0.4 µg of pCMVTnT-*Ror*β (for Figure S2A); 0 or 0.4 µg of pCMV-SPORT6-*Maff* (MGC clone # 30560, Invitrogen, for Figure S2B); 0 or 0.4 µg each of pMU2-*Eya3* and pMU2-*Six1* (for Figure 4B, E and F); 0, 0.133, 0.4 or 1.2 µg of pMU2-*Eya3* and 0 or 0.4 µg of pMU2-*Six1* (for Figure 4D); 0 or 0.4 µg each of pMU2-*Dbp* [19], pMU2-*Tef* and pMU2-*Hlf* (for Figure S2D); 0 or 0.4 µg each of pMU2-*Tef*, pMU2-*Hlf* and pMU2-*E4bp4* [19] (for Figure S2E); 0 or 0.4 µg each of pMU2-*Eya3*, pMU2-*Six1*, pMU2-*Tef* and pMU2-*Hlf* (for Figure S2H and J); 0, 0.133, 0.4 or 1.2 µg of pMU2-*Eya3* and 0 or 0.4 µg of pMU2-*Six1*, pMU2-*Tef* and pMU2-*Hlf* (for Figure S2I). Empty vector was used to bring the total amount of DNA to 4.0 µg per well. In addition, 50 ng of a phRL-SV40 plasmid (Renilla *Luciferase* (*RLuc*) reporter vector, Promega) was added to each transfection as an internal control for transfection efficiency. pGL4.13 (Promega) was used for the construction of the control promoter (P(SV40)). Forty-eight hours after the transfection, the cells were harvested and assayed with the Dual-Luciferase Reporter Assay System (Promega). The Luciferase activity was normalized to the RLuc activity.

Construction of Plasmids

pGL4.10-P(*TSH*β-7.7k)

A 7.7-kbp promoter region of the mouse *TSH*β gene was amplified from C57BL/6 genomic DNA using PCR with the following primers (Hokkaido System Science, restriction recognition sequences are underlined): Forward primer containing the *Xho*I recognition sequence, (5'-AAGCCTCGAGGTGGGTCTGGTGGATGACTGCTAAGAA-3'); reverse primer containing *EcoR*V recognition sequence, (5'-TTCTGATATCGGTAGACACCTACCTTACTTTGCATGAGTG-3'). The PCR product was digested with *Xho*I and *EcoR*V, and cloned into the *Xho*I-*EcoR*V site of a pGL4.10 vector (Promega) immediately upstream of *Luc2*, to obtain pGL4.10-P(*TSH*β-7.7k). *TSH*β promoter constructs were cloned at the +30 position because there is an MEF3 site at +1 position of *TSH*β

gene region (**Figure 4C**). We thus designed *TSH*β promoter constructs so that it covers a sufficient flanking sequence of the MEF3 site.

pCMVTnT-*Ror*β

The full-length coding sequence of mouse *Ror*β was amplified from an NIH3T3 cDNA library using PCR with the following primers: Forward primer, 5'-ATGCGAGCACAAATTGAAGTGATACC-3' (Hokkaido System Science); reverse primer, 5'-TCATTTGCAGACCGCAGCACAGTCAGG-3'. The PCR product was treated with the Mighty Cloning kit (TaKaRa) for 5'-end phosphorylation, and cloned into the *Sma*I sites of a pCMVTnT vector (Promega). The resulting construct was designated as pCMVTnT-*Ror*β. In this pCMVTnT vector, the gene is regulated by a CMV promoter.

pGL4.10-P(*TSH*β-0.6k), pGL4.10-P(*TSH*β-0.2k), and pGL4.10-P(*TSH*β-0.1k)

We used pGL4.10-P(*TSH*β-7.7k) plasmid DNA as a template for cloning the 0.6-, 0.2-, and 0.1-kbp promoter regions of *TSH*β. The 0.6-, 0.2-, and 0.1-kbp *TSH*β promoter regions were amplified, treated with the Mighty Cloning kit (TaKaRa) for 5'-end phosphorylation, and cloned into the *EcoR*V sites of a pGL4.10 vector (Promega). The resulting constructs were designated as pGL4.10-P(*TSH*β-0.6k), pGL4.10-P(*TSH*β-0.2k), and pGL4.10-P(*TSH*β-0.1k).

Oligonucleotide Sequences for Constructing the Shorter *TSH*β Promoters (Hokkaido System Science)

Cloning of P(*TSH*β-0.6k):

Forward primer: 5'-CCAAGACAGAATTTGATCTCAGGTCAGTT-3'

Reverse primer: 5'-CACTCTCCGTTCATTTTATACCCTTCA-3'

Cloning of P(*TSH*β-0.2k):

Forward primer: 5'-GATATGTTTCAAATAGAAGAGAGGAAG-3'

Reverse primer: 5'-CACTCTCCGTTCATTTTATACCCTTCA-3'

Cloning of P(*TSH*β-0.1k):

Forward primer: 5'-AGATGCTTTTCAGATAAGAAAGCAGC-3'

Reverse primer: 5'-CACTCTCCGTTCATTTTATACCCTTCA-3'

pMU2-*Eya3* and pMU2-*Six1*

The full-length coding sequences of mouse *Eya3* and *Six1* were amplified from the NIH3T3 cDNA library by PCR, using forward primers containing the *I-Sce*I recognition sequence and reverse primers containing the *PI-Psp*I recognition sequence (Hokkaido System Science, restriction recognition sequences are underlined). The PCR products were digested with *I-Sce*I

and *PI-Psp*I (New England BioLabs) and cloned into the pMU2 vector [20], and the resulting vectors were designated as pMU2-*Eya3* and pMU2-*Six1*. In these pMU2 vectors, the genes are regulated by a CMV promoter.

Oligonucleotide Sequences for the Cloning of *Eya3* and *Six1*

Cloning of *Eya3*:

Forward primer: 5'-ATTACCCTGTTATCCCTAATGAAGAAGAGCAAGAC CTACCAGAGC-3'

Reverse primer: 5'-ACCCATAATACCCATAATAGCTGTTTGCCATCAGAG GAAGTCAAGCTCTAAAGCC-3'

Cloning of *Six1*:

Forward primer: 5'-ATTACCCTGTTATCCCTAATTCGATGCTGCCGTCGT TTGGTT-3'

Reverse primer: 5'-ACCCATAATACCCATAATAGCTGTTTGCCAGGAACC CAAGTCCACCAAACTG-3'

pGL4.10-P(*TSH*β-ΔMEF3), pGL4.10-P(*TSH*β-mutMEF3), pGL4.10-P(*TSH*β-mutD), pGL4.10-P(*TSH*β-ΔSo1), and pGL4.10-P(*TSH*β-ΔSo2)

We used pGL4.10-P(*TSH*β-0.1k) as a template. The inverse PCR products were treated with the Mighty Cloning kit (TaKaRa) for 5'-end phosphorylation, and subsequently self-ligated. The constructs were designated as pGL4.10-P(*TSH*β-ΔMEF3), pGL4.10-P(*TSH*β-mutMEF3), pGL4.10-P(*TSH*β-mutD), pGL4.10-P(*TSH*β-ΔSo1), and pGL4.10-P(*TSH*β-ΔSo2).

Oligonucleotide Sequences for Constructing Mutated or Deleted *TSH*β Promoters (Hokkaido System Science)

Inverse PCR of pGL4.10-P(*TSH*β-ΔMEF3):

Forward primer: 5'-AGGGTATAAAATGAACGGAGAGTGG-3'

Reverse primer: 5'-AATTCCCCTCTGATCTTCTTG-3'

Inverse PCR of pGL4.10-P(*TSH*β-mutMEF3):

Forward primer: 5'-CATCTAGAGGGTATAAAATGAACGGAGAGTGG-3'

Reverse primer: 5'-AATTCCCCTCTGATCTTCTTG-3'

Inverse PCR of pGL4.10-P(*TSH*β-mutD):

Forward primer: 5'-CACCCGGCACAAGAAGATCAGAGGGGAATTATCCT G-3'

Reverse primer: 5'-TTGCATTCGAATTGCTGCTTTCTTATCTG-3'

Inverse PCR of pGL4.10-P(*TSH*β-ΔSo1):

Forward primer: 5'-GCAATTATATAAACAAGAAGATCAGAGG-3'

Reverse primer: 5'-TGCTTTCTTATCTGAAAAGCATCTATCC-3'

Inverse PCR of pGL4.10-P(*TSH*β-ΔSo2):

Forward primer: 5'-TTCGAATGCAATTATATAAACAAGAAGATC-3'

Reverse primer: 5'-TTATCTGAAAAGCATCTATCCTCGAG-3'

Author Contributions

H.R.U. and Y.S. designed the overall project. K.M., M.N., K.H., and Y.S. collected samples. K.D.U. performed the GeneChip and qPCR experiments. K.M., M.N., and K.T. performed the ISH experiments. T.K. designed and performed the computational analyses, and constructed the integrated database. M.U. performed the promoter assay. K.M., M.U., T.K., Y.S., and H.R.U. wrote the manuscript. All authors discussed the results and commented on the manuscript.

Supplemental References

1. Yoo, S.H., Yamazaki, S., Lowrey, P.L., Shimomura, K., Ko, C.H., Buhr, E.D., Siepka, S.M., Hong, H.K., Oh, W.J., Yoo, O.J., et al. (2004). PERIOD2::LUCIFERASE real-time reporting of circadian dynamics reveals persistent circadian oscillations in mouse peripheral tissues. Proc Natl Acad Sci U S A *101*, 5339-5346.
2. Guilding, C., Hughes, A.T., Brown, T.M., Namvar, S., and Piggins, H.D. (2009). A riot of rhythms: neuronal and glial circadian oscillators in the mediobasal hypothalamus. Mol Brain *2*, 28.
3. Dupre, S.M., Miedzinska, K., Duval, C.V., Yu, L., Goodman, R.L., Lincoln, G.A., Davis, J.R., McNeilly, A.S., Burt, D.D., and Loudon, A.S. (2010). Identification of Eya3 and TAC1 as long-day signals in the sheep pituitary. Curr Biol *20*, 829-835.
4. Alon, U. (2007). An introduction to systems biology: design principles of biological circuits. In Network Motifs in Developmental, Signal Transduction, and Neuronal Networks. (London: Chapman & Hall/CRC), pp. 97-129.
5. Drolet, D.W., Scully, K.M., Simmons, D.M., Wegner, M., Chu, K.T., Swanson, L.W., and Rosenfeld, M.G. (1991). TEF, a transcription factor expressed specifically in the anterior pituitary during embryogenesis, defines a new class of leucine zipper proteins. Genes Dev *5*, 1739-1753.
6. Mueller, C.R., Maire, P., and Schibler, U. (1990). DBP, a liver-enriched transcriptional activator, is expressed late in ontogeny and its tissue specificity is determined posttranscriptionally. Cell *61*, 279-291.
7. Inaba, T., Roberts, W.M., Shapiro, L.H., Jolly, K.W., Raimondi, S.C., Smith, S.D., and Look, A.T. (1992). Fusion of the leucine zipper gene HLF to the E2A gene in human acute B-lineage leukemia. Science *257*, 531-534.
8. Cowell, I.G., Skinner, A., and Hurst, H.C. (1992). Transcriptional repression by a novel member of the bZIP family of transcription factors. Mol Cell Biol *12*, 3070-3077.
9. Zhang, W., Zhang, J., Kornuc, M., Kwan, K., Frank, R., and Nimer, S.D. (1995). Molecular cloning and characterization of NF-IL3A, a transcriptional activator of the human interleukin-3 promoter. Mol Cell Biol *15*, 6055-6063.
10. Kel, O.V., Romaschenko, A.G., Kel, A.E., Wingender, E., and Kolchanov, N.A. (1995). A compilation of composite regulatory elements affecting gene transcription in vertebrates. Nucleic Acids Res *23*, 4097-4103.
11. Ono, H., Hoshino, Y., Yasuo, S., Watanabe, M., Nakane, Y., Murai, A., Ebihara, S., Korf, H.W., and Yoshimura, T. (2008). Involvement of thyrotropin in photoperiodic signal transduction in mice. Proc Natl Acad Sci U S A *105*, 18238-18242.

12. Yoshimura, T., Nishio, M., Goto, M., and Ebihara, S. (1994). Differences in circadian photosensitivity between retinally degenerate CBA/J mice (rd/rd) and normal CBA/N mice (+/+). J Biol Rhythms *9*, 51-60.
13. Yoshimura, T., and Ebihara, S. (1996). Spectral sensitivity of photoreceptors mediating phase-shifts of circadian rhythms in retinally degenerate CBA/J (rd/rd) and normal CBA/N (+/+)mice. J Comp Physiol A *178*, 797-802.
14. Chatfield, C. (1996). The analysis of time series: An introduction, (London: Chapman & Hall/CRC).
15. Storey, J.D., and Tibshirani, R. (2003). Statistical significance for genomewide studies. Proc Natl Acad Sci U S A *100*, 9440-9445.
16. Ueda, H.R., Chen, W., Minami, Y., Honma, S., Honma, K., Iino, M., and Hashimoto, S. (2004). Molecular-timetable methods for detection of body time and rhythm disorders from single-time-point genome-wide expression profiles. Proc Natl Acad Sci U S A *101*, 11227-11232.
17. Minami, Y., Kasukawa, T., Kakazu, Y., Iigo, M., Sugimoto, M., Ikeda, S., Yasui, A., van der Horst, G.T., Soga, T., and Ueda, H.R. (2009). Measurement of internal body time by blood metabolomics. Proc Natl Acad Sci U S A *106*, 9890-9895.
18. Shigeyoshi, Y., Taguchi, K., Yamamoto, S., Takekida, S., Yan, L., Tei, H., Moriya, T., Shibata, S., Loros, J.J., Dunlap, J.C., et al. (1997). Light-induced resetting of a mammalian circadian clock is associated with rapid induction of the mPer1 transcript. Cell *91*, 1043-1053.
19. Kumaki, Y., Ukai-Tadenuma, M., Uno, K.D., Nishio, J., Masumoto, K.H., Nagano, M., Komori, T., Shigeyoshi, Y., Hogenesch, J.B., and Ueda, H.R. (2008). Analysis and synthesis of high-amplitude Cis-elements in the mammalian circadian clock. Proc Natl Acad Sci U S A *105*, 14946-14951.
20. Ukai, H., Kobayashi, T.J., Nagano, M., Masumoto, K.H., Sujino, M., Kondo, T., Yagita, K., Shigeyoshi, Y., and Ueda, H.R. (2007). Melanopsin-dependent photo-perturbation reveals desynchronization underlying the singularity of mammalian circadian clocks. Nat Cell Biol *9*, 1327-1334.